Fraunhofer

IAPT

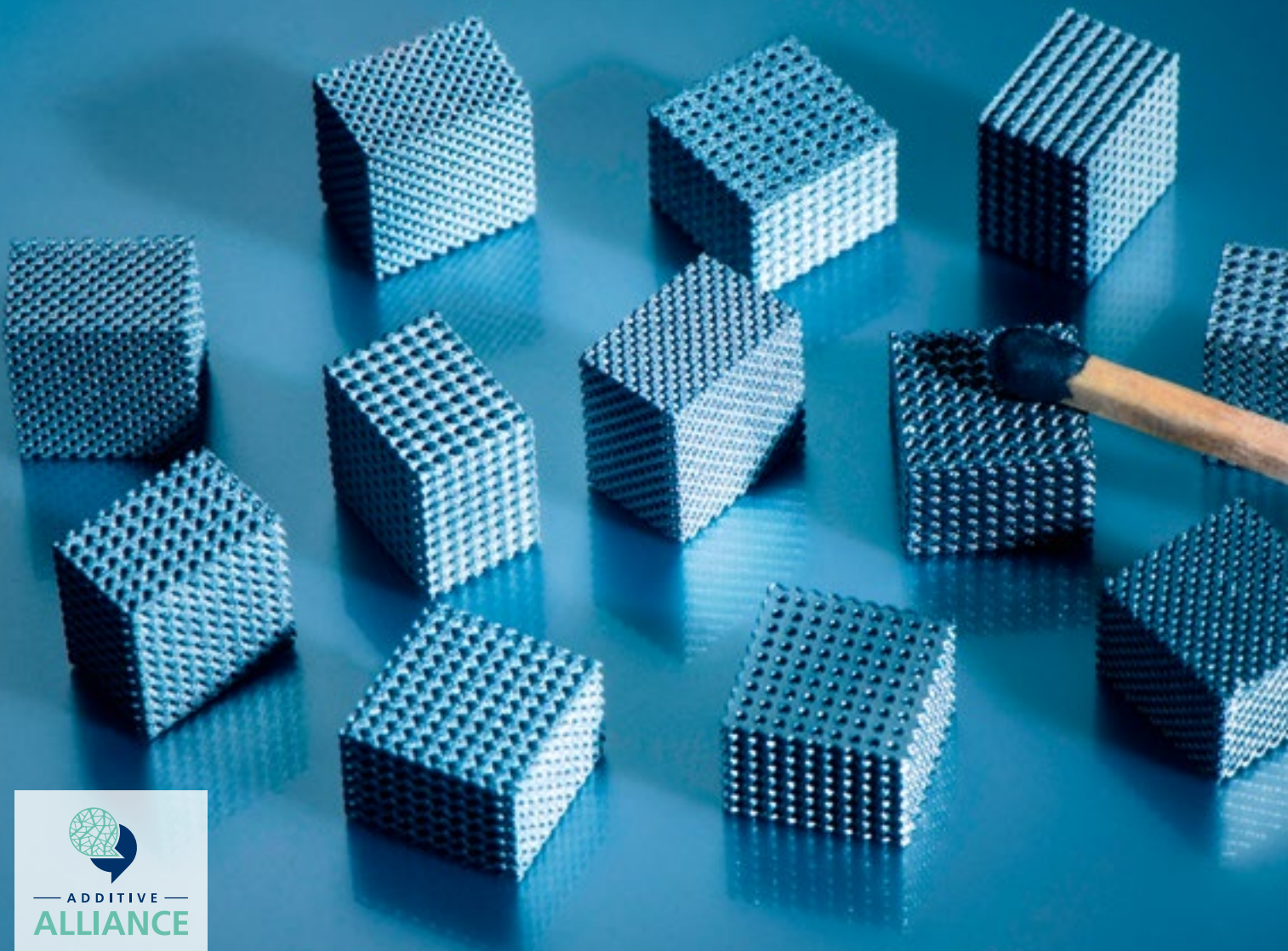**FRAUNHOFER RESEARCH INSTITUTION FOR ADDITIVE MANUFACTURING TECHNOLOGIES IAPT**

APPLICATION POTENTIAL OF STRUCTURES BASED ON TRIPLY PERIODIC MINIMAL SURFACES

ADDITIVE ALLIANCE

Contact

Fraunhofer Research Institution for
Additive Manufacturing Technologies IAPT

Am Schleusengraben 14
21029 Hamburg-Bergedorf
Germany

Telephone +49 40 48 40 10-500

info@iapt.fraunhofer.de

www.iapt.fraunhofer.de

www.linkedin.com/company/fraunhofer-iapt

www.youtube.com/FraunhoferIAPT

APPLICATION POTENTIAL OF STRUCTURES BASED ON TRIPLY PERIODIC MINIMAL SURFACES (TPMS)

Based on selected scientific literature, this report offers assistance in selecting a suitable TPMS structure to fulfill a technical function (for example shock, vibration, acoustics, heat transfer and the medical field). The graphic below outlines the basic procedure exemplified by the selection of a TPMS structure for the stem of a finger joint implant.

POSSIBLE FUNCTIONS OF TPMS

AVAILABLE TPMS STRUCTURES

PROPERTIES OF TPMS STRUCTURES

WELL-FOUNDED SELECTION OF TPMS

2_CONTENT

3_ACKNOWLEDGEMENT

Deep Dives are reports intended exclusively for the members of the Additive Alliance®. They provide latest insights into the science behind additive manufacturing (AM). Our gratitude goes to the following members. This Deep Dive could not have been prepared without their financial support.
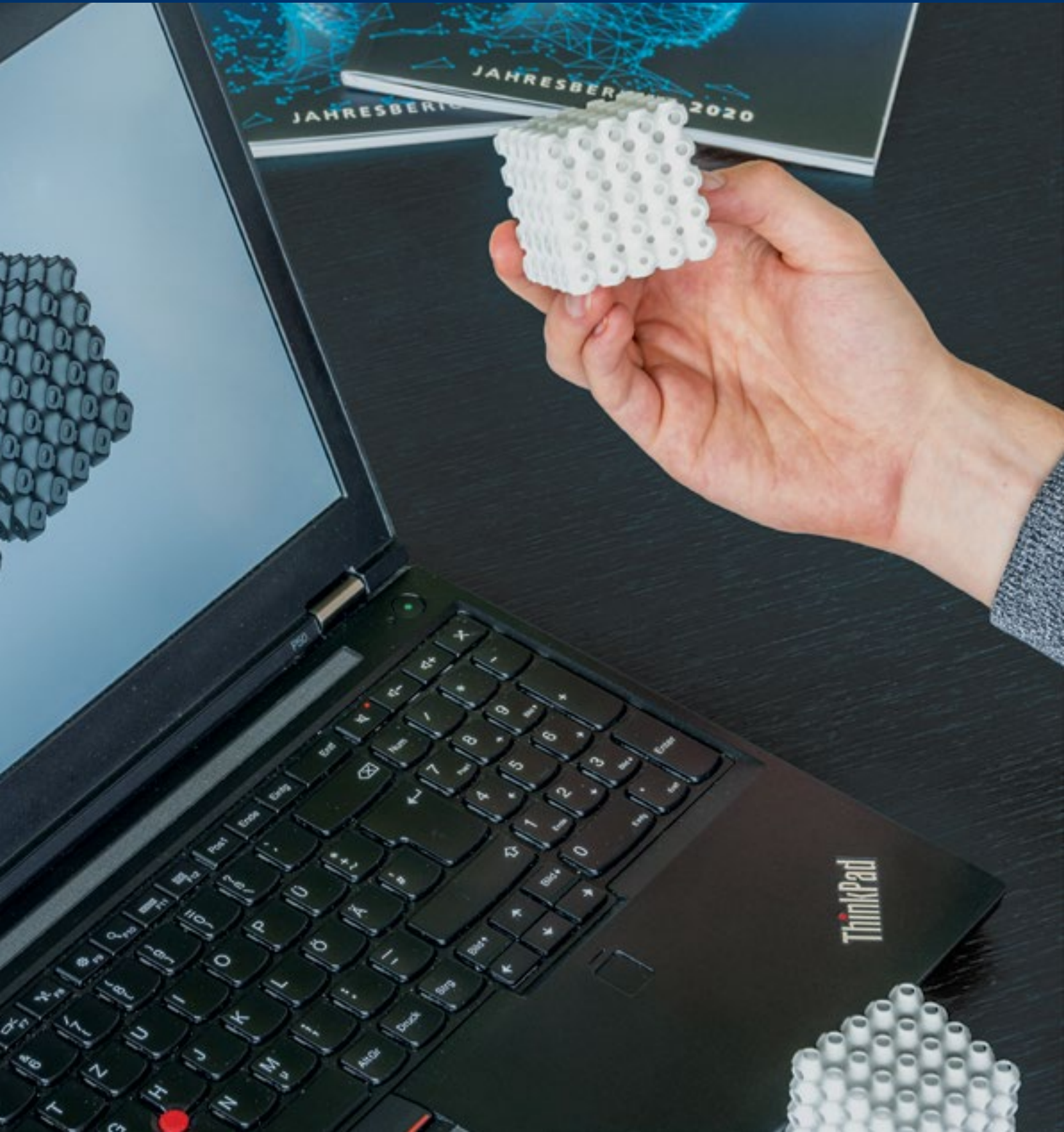
4_ABOUT THE AUTHORS

With this work, the authors want to provide an insight into the world of structures based on TPMS. These structures have outstanding properties with regard to a wide range of functions, such as heat transfer, for example. Additive manufacturing and modern modeling tools allow engineers to take advantage of these properties.

The lead author of this Deep Dive is Arthur Seibel, head of the Bionic Function and Design group. However, the entire group was involved in developing the content, thus making it possible to compile and process the accumulated expert knowledge on the individual functions and the benefits of TPMS structures.

Arthur Seibel, *Dr.-Ing. habil. Dipl.-Ing.*
Head of Bionic Function and Design

Heiko Blunk, *M. Sc.*
Michael Lippert, *M. Eng.*
Yannick Löw, *M. Sc.*
Yanik Senkel, *M. Sc.*
Felix Weigand, *M. Sc.*

Please do not hesitate to contact our team with any questions:

Arthur Seibel
Telephone +49 40 48 40 10-748
arthur.seibel@iapt.fraunhofer.de
https://www.iapt.fraunhofer.de/de/kompetenzbereiche/am-design.html

5_MOTIVATION

Structures based on TPMS exhibit physical properties that are superior to other lattice types, such as strut-based lattice structures, for example. Among others, advantageous properties include a high stiffness-to-weight ratio and a high surface-to-volume ratio, as well as a mathematically smooth geometry that avoids peak loads.

Due to their many advantages, TPMS structures have also evolved in nature, where they can be found fulfilling different functions in various organisms. Interesting manifestations can be seen particularly in sea urchins, butterfly wing scales and exoskeletons of various beetle species [Han18]. An example is shown in Figure 1.
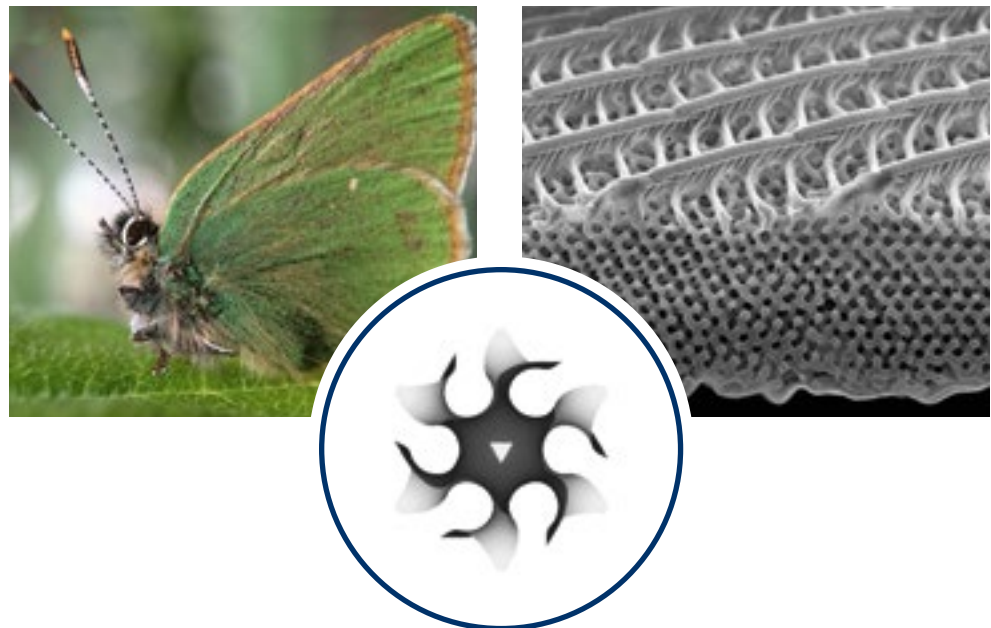
Figure 1: Butterfly wing scales of the species C. rubi. based on a gyroid structure [Cor17]

Advances in manufacturing technologies, especially in additive manufacturing, and software development facilitate the design and implementation of such structures in real products.

This Deep Dive is intended to provide an overview of mathematical and physical properties of TPMS structures and outline potential applications in different technological fields. It also provides methodological tools (in the form of diagrams and tables) at appropriate points so that engineers can select a TPMS structure suitable for their specific application.

6_APPROACH OF THE DEEP DIVE

For this Deep Dive, we performed a literature review of TPMS structures and the corresponding applications. We also conducted research on appropriate CAD software for mathematical visualization and included our own investigations where necessary.

In terms of applications, the main focus is always on providing a methodology for selecting appropriate TPMS-based geometries. Figure 2 presents an overview of the application areas and the corresponding key questions addressed in this Deep Dive.

Shock:
Why can TPMS structures be beneficial in controlled impact energy absorption?

Vibration:
Which TPMS structure can be used to decouple a vibrating system?

Acoustics:
Which TPMS structure can be used for proper sound absorption?

Heat transfer:
Which TPMS structure can be used to achieve a desired heat transfer or heat exchange?

Medical:
Why can TPMS structures be beneficial in bone scaffold and implant design?

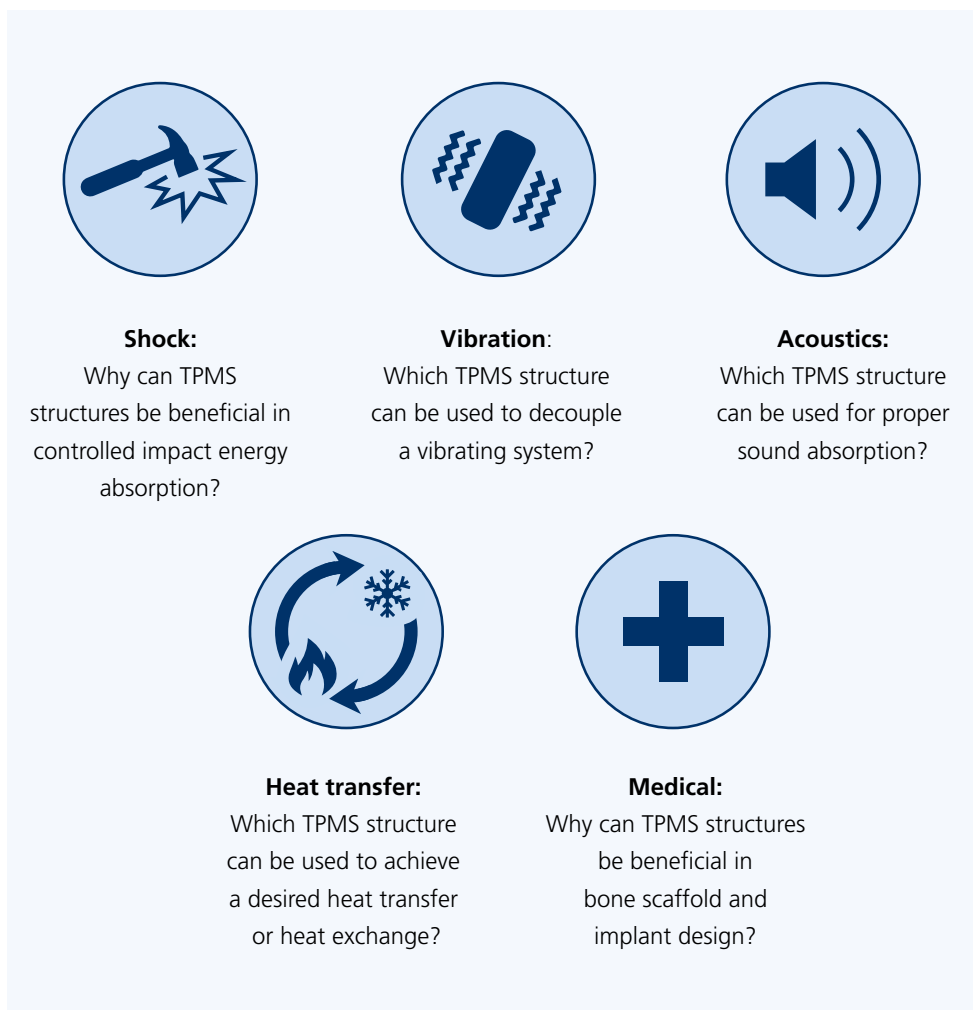*Figure 2: Overview of the application areas featured in this report*

6.1_GEOMETRICAL STRUCTURE

TPMS locally minimize their area for a given boundary so that the mean curvature at any point on the surface is zero. TPMS can be considered as periodically arranged unit cells with the following properties:

• They are mathematically smooth,
• have no sharp corners or edges,
• divide the space into two nonintersecting, intertwined domains, and
• can usually be described by one implicit equation.

After mathematically defining a TPMS, a volume can be created by thickening the surface in both normal directions. This kind of TPMS structure is called a shell structure. The larger the wall thickness that is chosen, the greater the achieved relative density[*] of the structure. Figure 3 shows some selected examples of TPMS shell structures. An alternative to shell structures are solid structures. These are formed when one of the two subdomains created by the minimal surface area is considered a solid, while the other subdomain remains void. However, solid TPMS structures are used much less frequently due to their poorer mechanical properties compared to TPMS shell structures [AlK19].

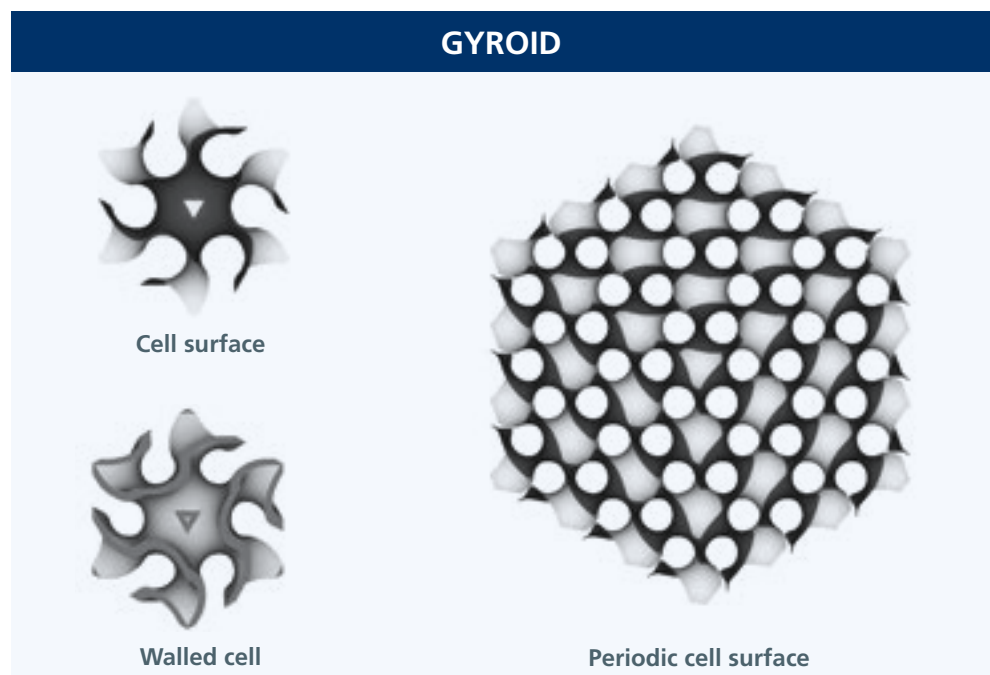[*]Ratio of solid material to total volume; also denoted as volume fraction.
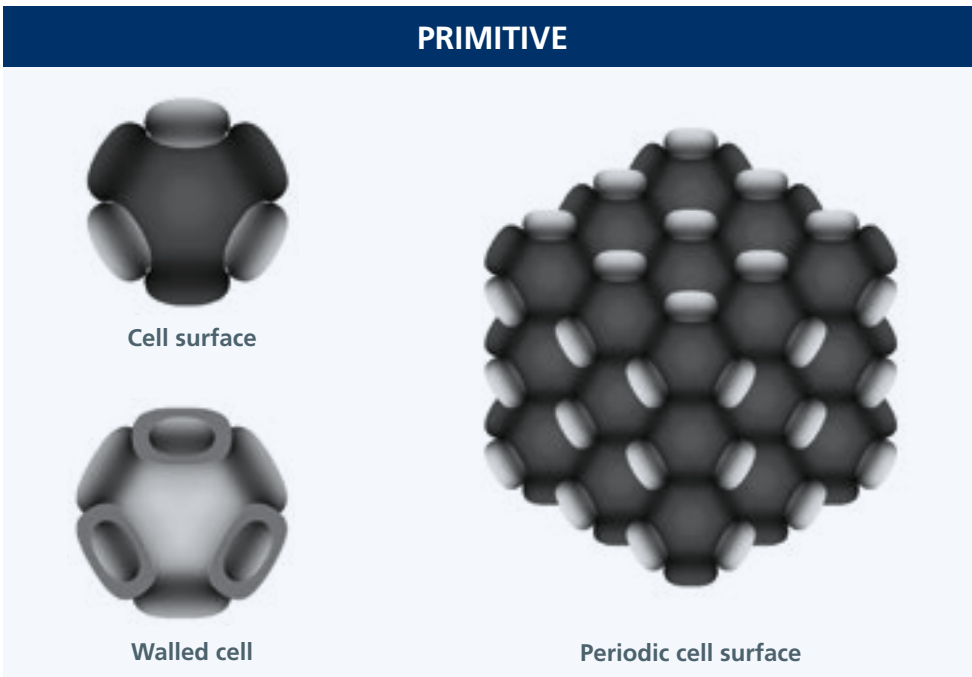
GYROID

Cell surface

Walled cell

Periodic cell surface

Figure 3: Overview of selected TPMS shell structures

PRIMITIVE

Cell surface

Walled cell

Periodic cell surface

Figure 3: Overview of selected TPMS shell structures (cont.)

DIAMOND

Cell surface

Walled cell

Periodic cell surface

Figure 3: Overview of selected TPMS shell structures (cont.)

SPLIT P

Cell surface

Walled cell

Periodic cell surface

NEOVIUS

Cell surface

Walled cell

Periodic cell surface

LIDINOID

Cell surface

Walled cell

Periodic cell surface

Figure 3: Overview of selected TPMS shell structures (cont.)

IWP

Cell surface

Walled cell

Periodic cell surface
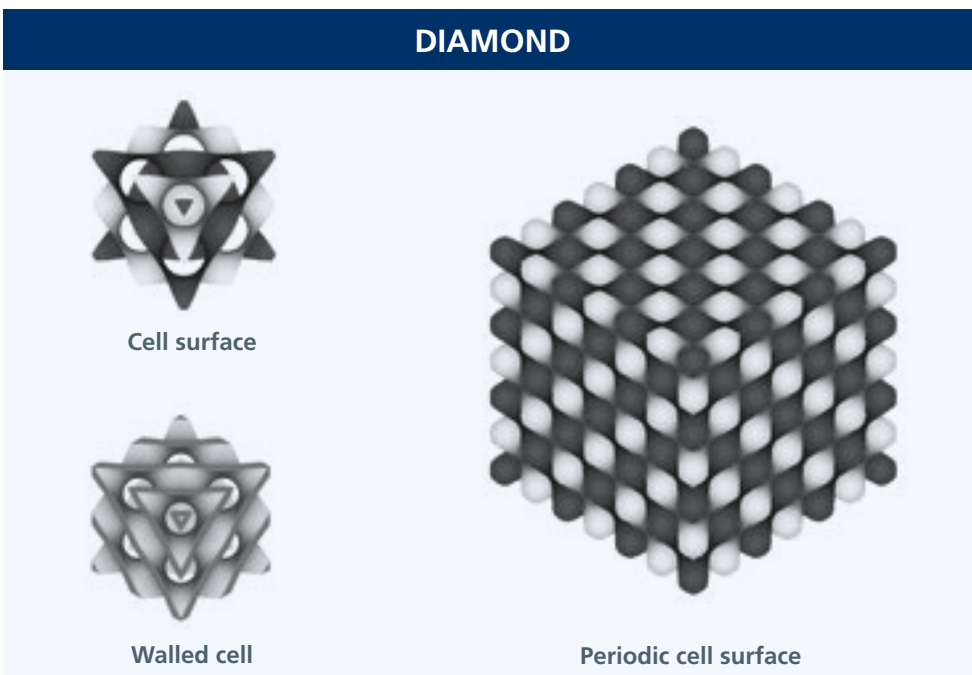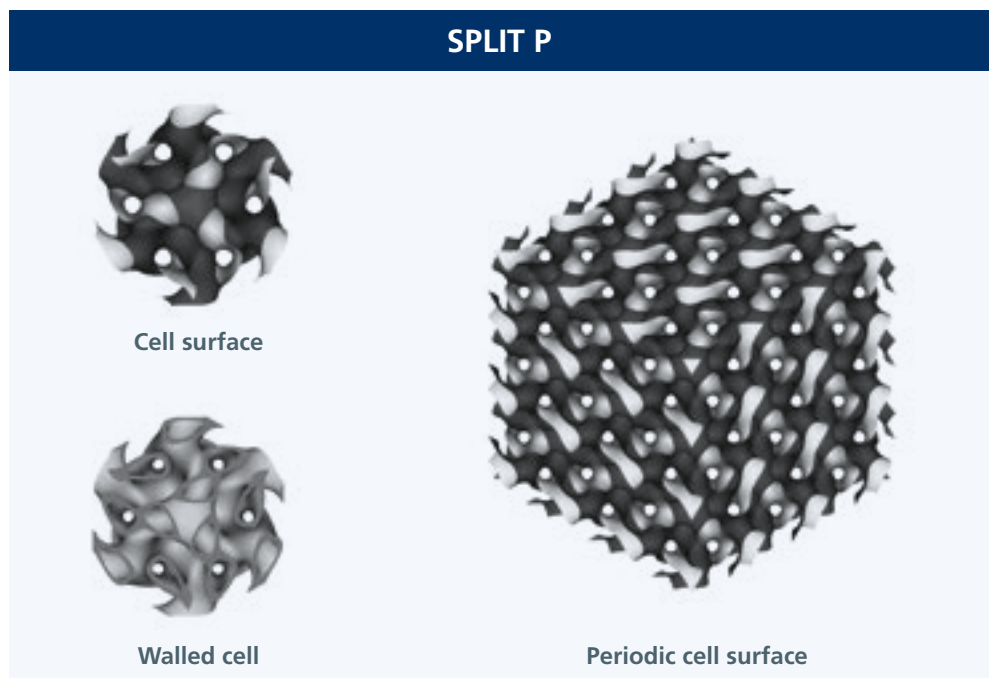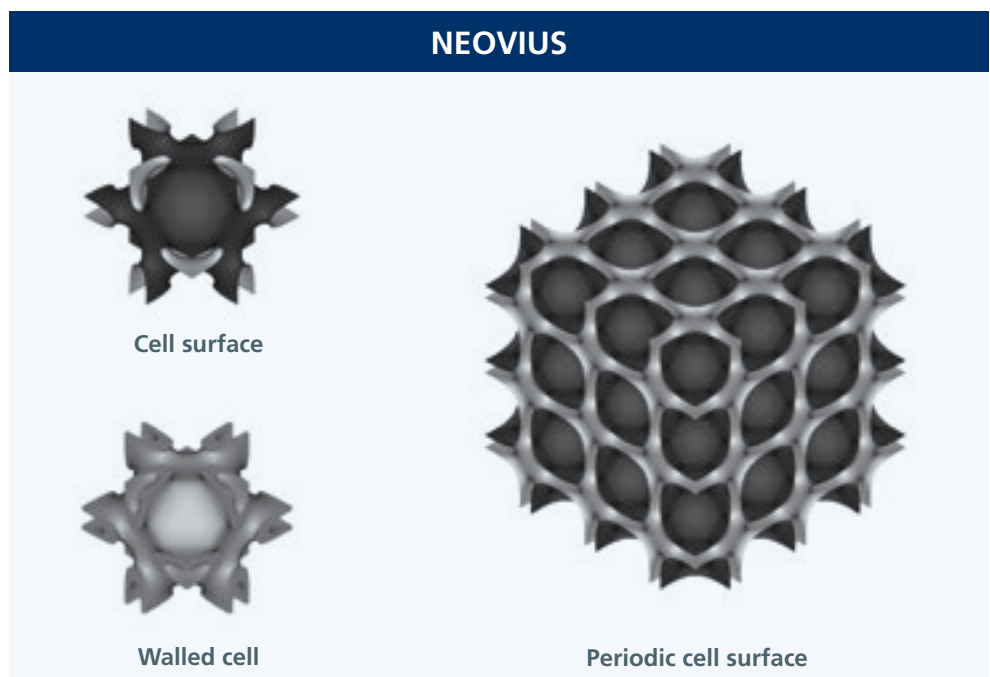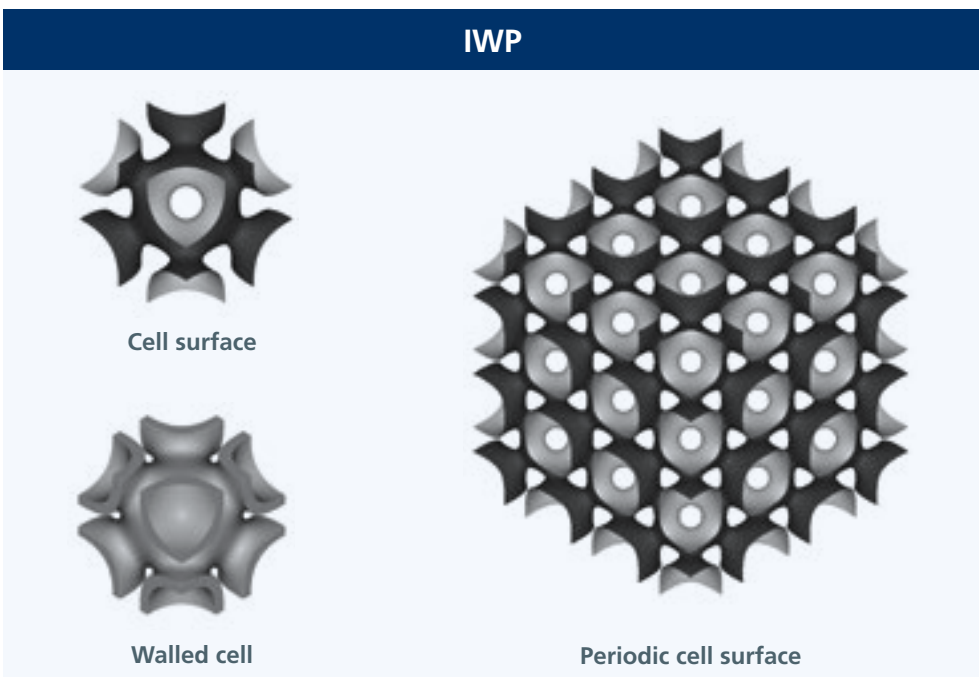
Figure 3: Overview of selected TPMS shell structures (cont.)

FISCHER-KOCH S

Cell surface

Walled cell

Periodic cell surface

FFigure 3: Overview of selected
TPMS shell structures (cont.)

FRD

Cell surface

Walled cell
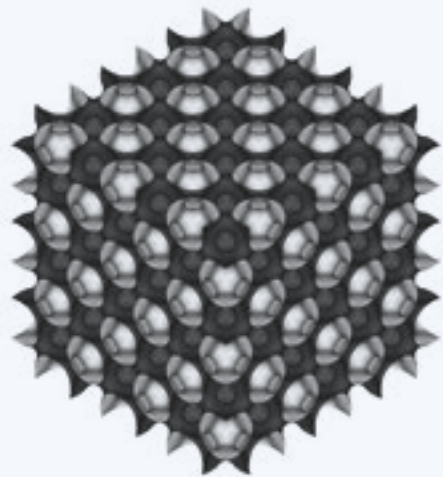
Periodic cell surface

Figure 3: Overview of selected
TPMS shell structures (cont.)

KP

Cell surface

Walled cell

Periodic cell surface

Figure 3: Overview of selected TPMS shell structures (cont.)

PN
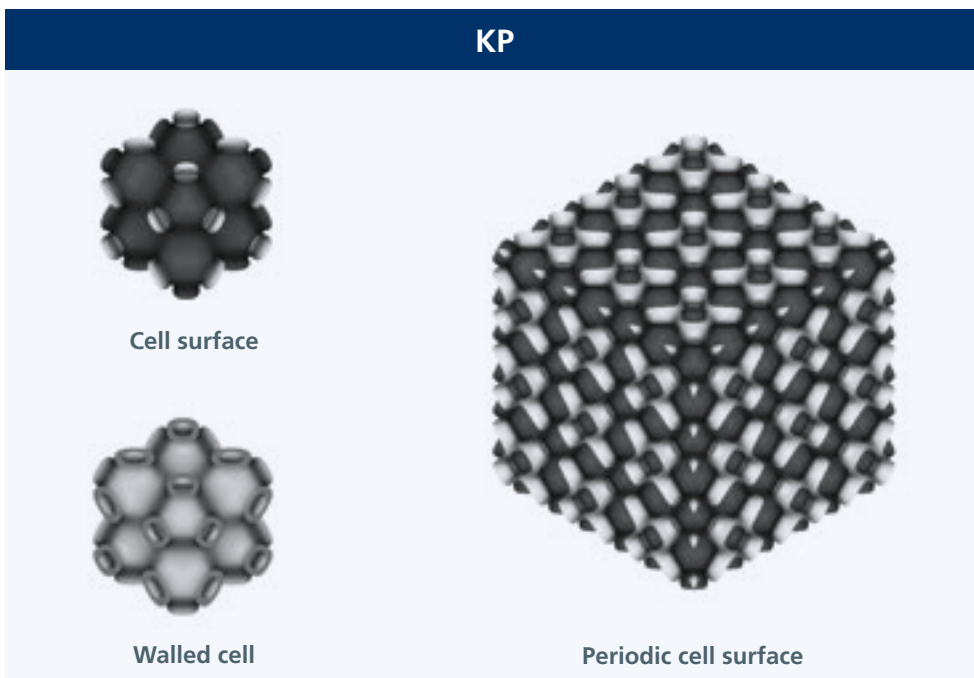
Cell surface

Walled cell

Periodic cell surface
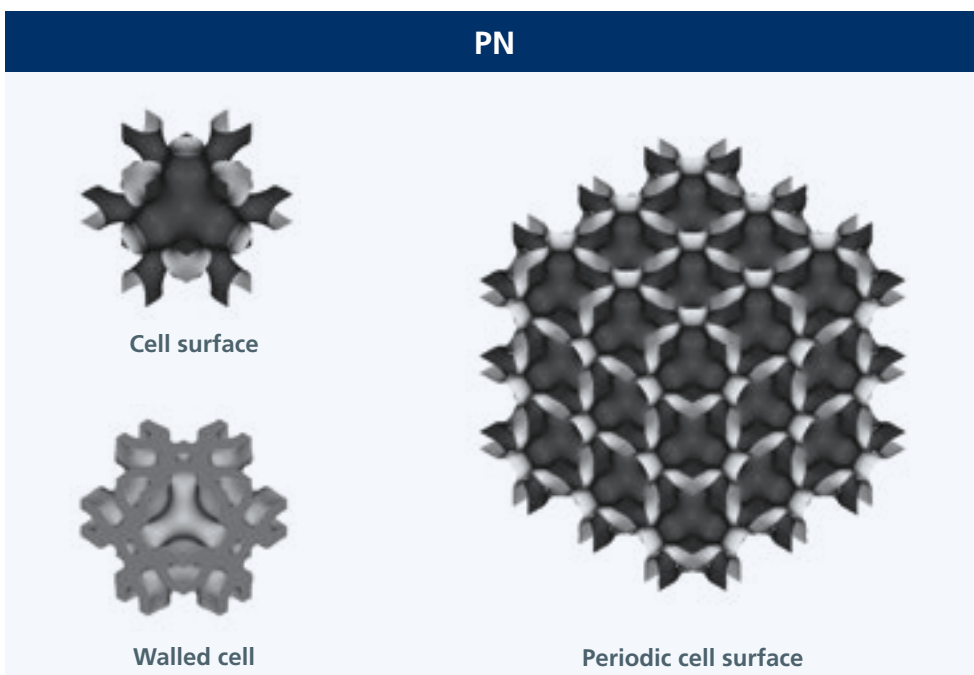
Figure 3: Overview of selected TPMS shell structures (cont.)

DOUBLE GYROID

Cell surface

Walled cell

Periodic cell surface

Figure 3: Overview of selected TPMS shell structures (cont.)

DOUBLE PRIMITIVE

Cell surface
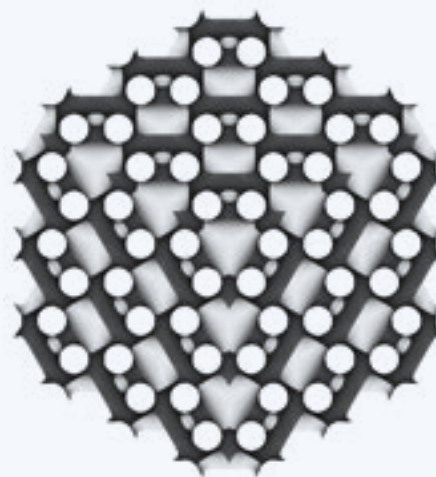
Walled cell

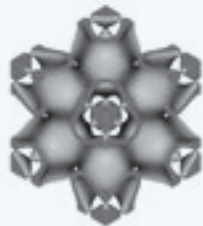**Periodic cell surface**

Figure 3: Overview of selected TPMS shell structures (cont.)

DOUBLE DIAMOND 1

Cell surface

Walled cell
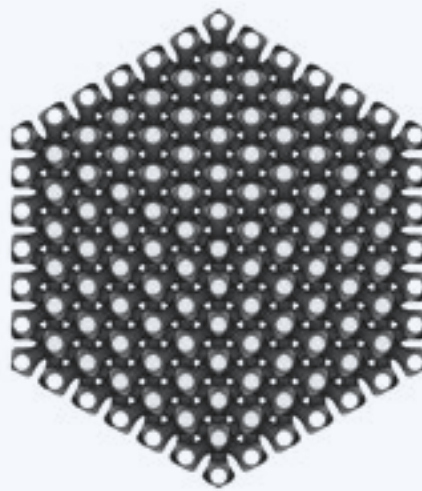
Periodic cell surface

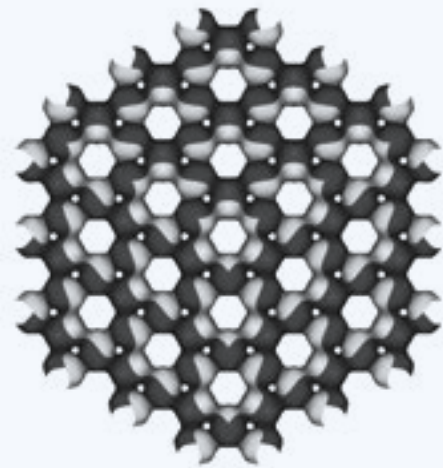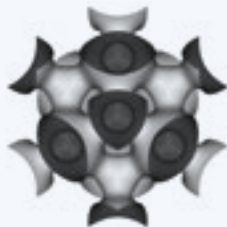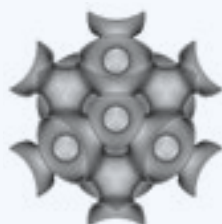*Figure 3: Overview of selected TPMS shell structures (cont.)*

DOUBLE DIAMOND 2

Cell surface
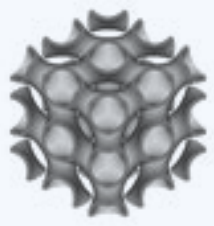
Walled cell
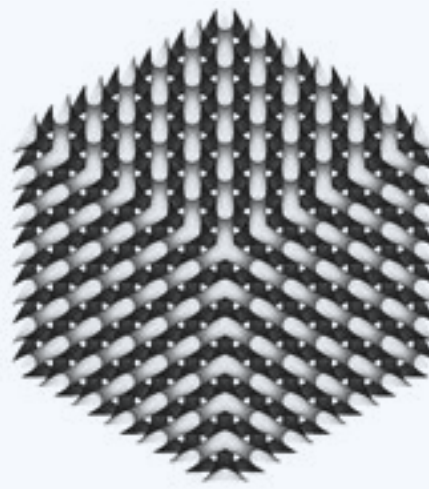
Periodic cell surface

Figure 3: Overview of selected TPMS shell structures (cont.)

6.2_POSSIBLE ADAPTATIONS

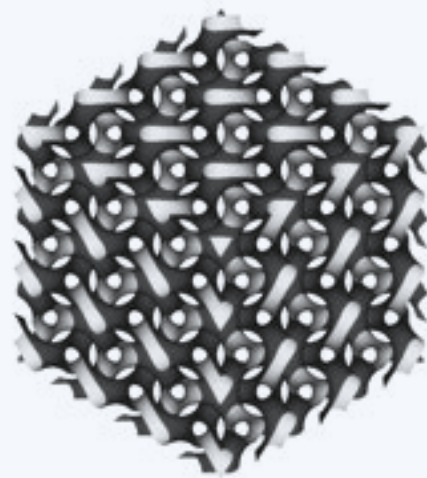Besides setting cell size and wall thickness as the structural parameters, grading TPMS structures offers further design options that influence the physical properties of the structures. In this context it is possible to make a distinction between the following three types (see Figure 4 for examples):

- In cell size grading, the cell size of the TPMS structure is continuously increased or reduced. Here, the relative density remains constant.
- In wall thickness grading, the wall thickness of the TPMS structure is continuously increased or reduced, allowing targeted narrowing or widening of the channels. Here, the relative density increases with increasing wall thickness.
- In bias grading, the surfaces of the TPMS structure can be continuously shifted toward one of the subdomains (by adjusting the bias parameter in the mathematical equation). This distortion of the TPMS structure creates channels that become continuously narrower, up to closure. Bias grading can be used to adjust the density of the cells.

Furthermore, the TPMS structure can be transformed, that is, the periodic arrangement of the TPMS can be transferred into another mathematical space (e.g. from Cartesian to polar coordinates). Circular or spherical arrangements can be created in this way, for example.

CELL SIZE GRADING
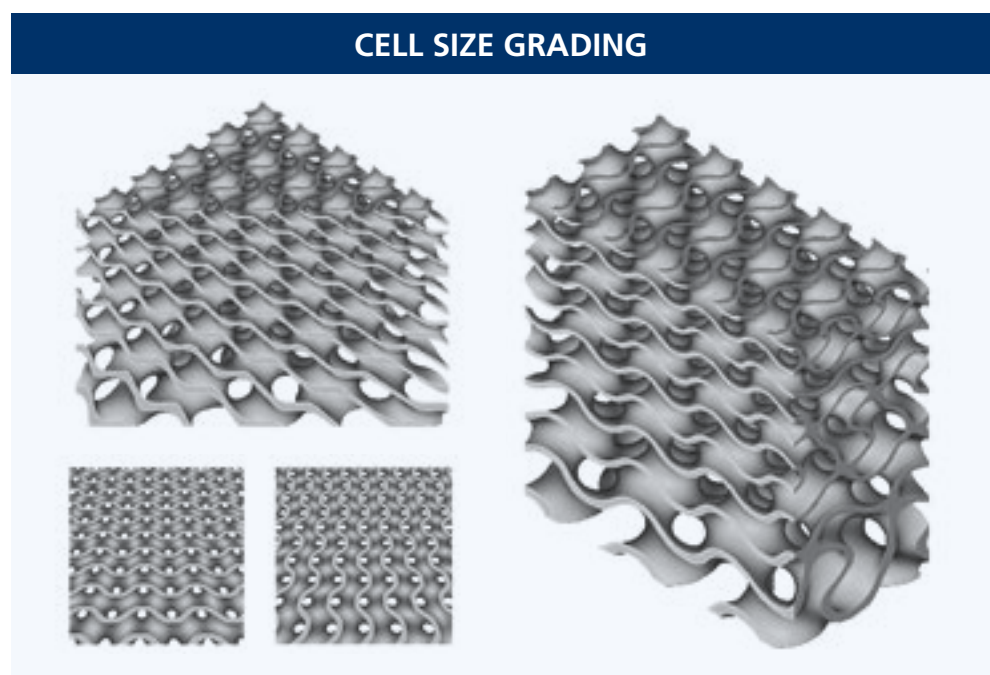
Figure 4: Examples of different types of grading of the shelled gyroid structure

WALL THICKNESS GRADING
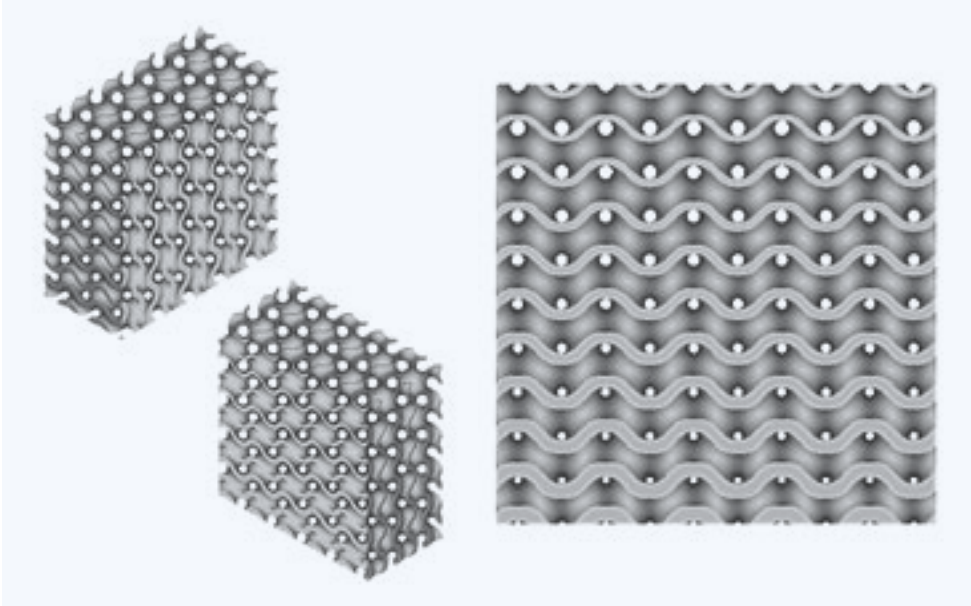
Figure 4: Examples of different types of grading of the shelled gyroid structure (cont.)

BIAS GRADING
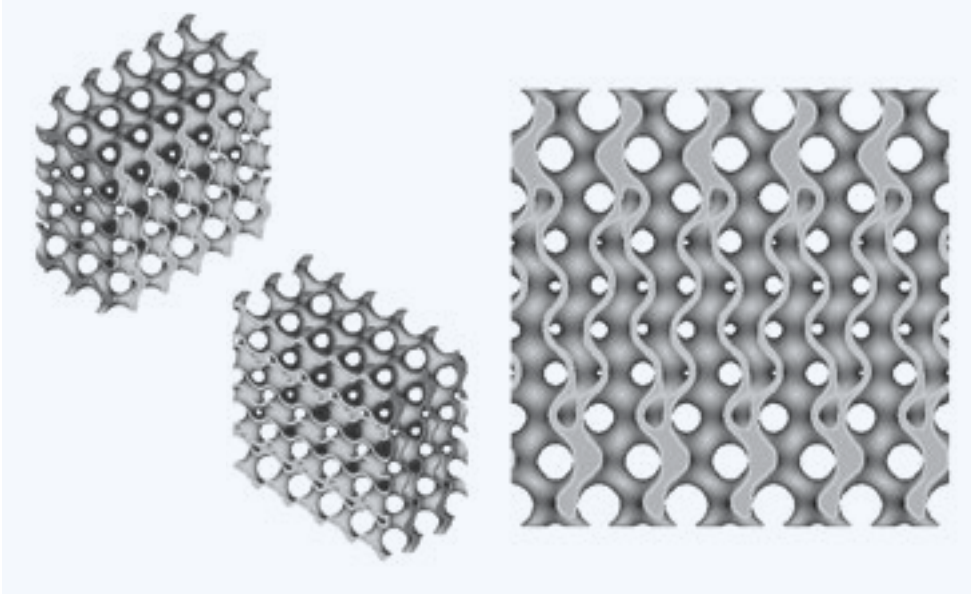
Figure 4: Examples of different types of grading of the shelled gyroid structure (cont.)

6.3_GEOMETRIC MODELING

TPMS structures largely exploit the potential of additive manufacturing in terms of design complexity and resolution. However, as designs become more complex, the demands made of software and hardware also increase. Various approaches have therefore been developed in recent years to create components with TPMS geometries. Figure 5 shows an overview of approaches that can currently be used in various software in the industrial environment.

Similar to strut-based lattice modeling, unit cells of TPMS can be defined and arranged in a periodical 3D pattern. Two different methods are used to model a unit cell. The first method is implemented using a classical CAD system, in which the unit cell is modeled as a boundary representation (B-rep) using (3D) sketches. If necessary, the surfaces are defined section by section

TPMS DESIGN METHODS

B-REP-BASED UNIT CELL	MESH-BASED UNIT CELL	DIRECT IMPLICIT MODELING

(3D) Sketches / **Implicit mathematical description**

B-rep surface unit cell	B-rep surface unit cell	Mesh volume unit cell	Grading/ transforming	Grading/ transforming
Pattern array	Volume surface cell	Pattern array	Mesh	Bool. operations
Volume model	Pattern array	Bool. operations	Bool. operations	Mesh
Bool. operations	Bool. operations			

Data preperation

Figure 5: Schematic overview of relevant design methods for TPMS structures

and joined together. In the following, a solid model of the unit cell must be derived from the surfaces, the unit cell must be arranged in a periodical pattern, and the TPMS structure must be adapted to the part geometry using Boolean operations. The sequence of the last three steps can also be changed depending on the CAD system.

The second method for modeling TPMS is by implicit mathematical description. One possibility here is to calculate a mesh representation of the unit cell from the implicit mathematical definition of the TPMS structure. This unit cell can then be arranged periodically and combined with other geometries using Boolean operations.

Geometric complexity poses limitations on using unit cell-based approaches and especially B-rep-based approaches. On the one hand, CAD operations and visualization of the B-rep geometry models are accompanied by very high hardware requirements. On the other hand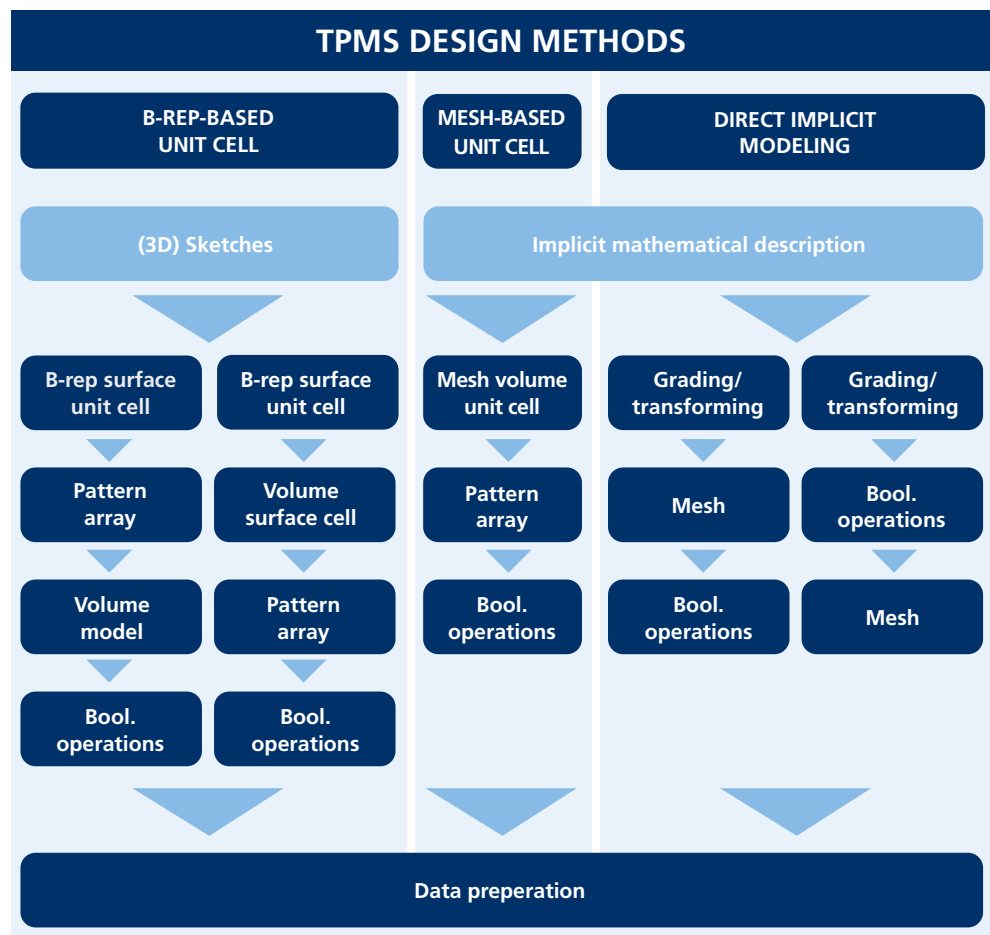, many CAD operations, such as Boolean operations, fillets, transitions, etc., are not robust in this scenario and consequently lead to errors [Sav19].

Unit cell-based approaches in the available software are also limited with regard to design possibilities. Here, TPMS structures cannot be graded in accordance with functional requirements as well as transformation/distortion of the TPMS structure, that is conformal alignment of the scaffold to a macro geometry.

Table 1 summarizes the features, advantages and disadvantages of different TPMS design methods.

	B-REP-BASED UNIT CELL	MESH-BASED UNIT CELL	IMPLICIT MODELING
B-rep design via splines, surfaces, etc.	●		
Pattern of previously designed unit cell (mesh)		●	
Design by mathematical formula			●
Design effort	high	medium	low
Software stability with high number of TPMS	low	medium	high

Table 1: Features, advantages and disadvantages of the different design methods

| 23

Comprehensive adaptation and design freedom in industrially usable software is currently only possible through direct implicit modeling. Here, all adaptations are applied to the implicit mathematical description of the TPMS structure. Transfer into net or CAD formats only happens at the end of the design process. Beside the enormous design possibilities, the relatively low hardware resources and the robustness of the geometric operations must also be mentioned. Table 2 provides an overview of specialized software for component design with TPMS.

COMPANY	SOFTWARE	MESH-BASED UNIT CELL	IMPLICIT MODELING
CT CoreTechnologie GmbH	4D_Additive	●	
Materialise NV	3-matic / Magics	●	
3D Systems, Inc.	3DXpert	●	●*
Gen3D ltd.	Gen3D	●	●
Siemens Digital Industries Software	Siemens NX	●	●
nTopology, Inc.	nTopology		●

*This function is available as of software version V17.

Table 2: Possible software solutions for the specialized creation of TPMS

6.4_MANUFACTURABILITY

Conventional methods for manufacturing TPMS structures include physical vapor deposition, chemical vapor deposition, plasma spraying, powder metallurgy and layer-by-layer casting with thermal die casting. Most of these processes impose many limitations on product design and cannot produce components with high geometric fit, excellent accuracy, and expected mechanical properties. Recently, additive manufacturing has emerged as the most promising method for fabricating TPMS structures with complex external shapes and well-defined internal connections, as it offers far greater freedom in manufacturing [Yu19].

TPMS structures can be produced basically with any additive manufacturing process. So far, examples of powder bed, photopolymerization, material extrusion and jetting processes can be found in the literature [AlK19]. In powder bed processes, for example, particular care must be taken to ensure that the cell size is not too small to allow the unfused powder to be removed from the cavities, but also not too large to counteract potential dross formation and similar. Information on the manufacturable cell sizes depends on the process and the material and cannot be generalized but must be determined individually for each combination.

Every TPMS structure has interconnected channels with a minimum diameter. This is denoted as pore size and is a decisive factor in the manufacturability of TPMS-based structures. Pore size

GYROID	PRIMITIVE	DIAMOND

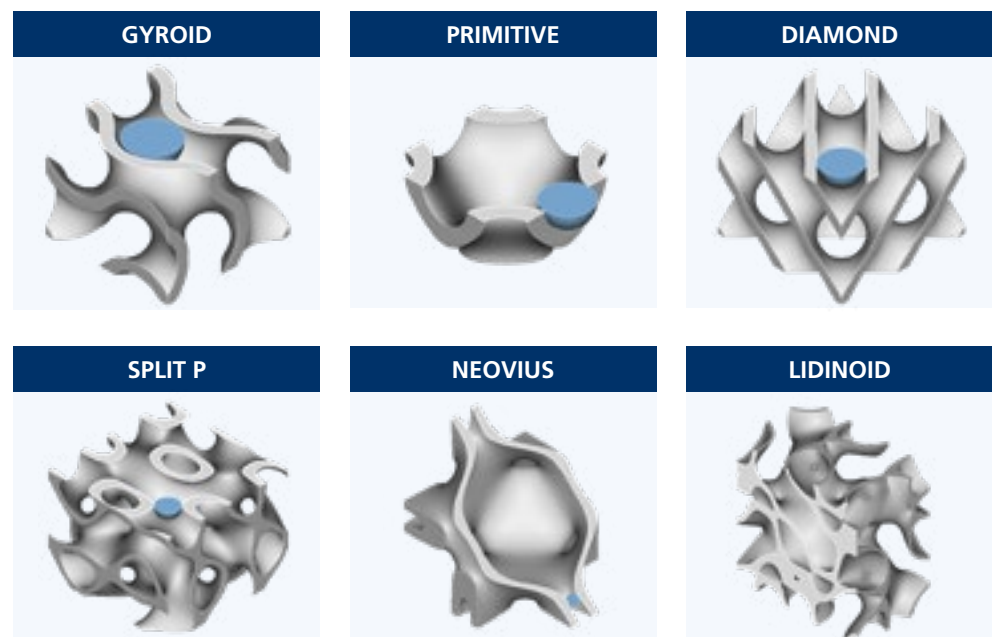| SPLIT P	NEOVIUS	LIDINOID

Figure 6: Selected TPMS shell structures with a relative density of 25% and a cell size of 10 mm. The largest diffusible sphere is illustrated in blue.

indicates the diameter of the largest sphere that could diffuse through the structure without getting stuck. Figure 6 illustrates this principle for six selected TPMS structures. Of the six structures shown, only the gyroid, primitive, and diamond structures are seen to be suitable for creating small structures due to the sufficiently large diameter of the largest diffusible sphere.

A relatively new additive manufacturing process is sinter-based metal binder jetting [Mun18], which has not yet been examined in the literature in the context of TPMS. The high resolution of binder jetting systems makes it possible to create cavities in the order of a few hundred micrometers. However, the size and length limits depend on powder removal, which in turn is dependent on the powder size itself in relation to the size and length of the cavities.

Since the parts first have to be unpacked after the printing process and then debinded before sintering, the green bodies are very brittle, which greatly limits the possibilities for powder removal. For this reason, a manufacturing study on selected TPMS shell structures was carried out to determine minimum cell sizes that can still be depowdered by manual means. The material used was 316L stainless steel.

In our experiments, depowdering was carried out manually using compressed air. Great care is required, since the samples have only a fraction of their final strength at this point. The presence of any unwanted residual powder left in the structure can be assessed by weighing the green parts and comparing them with their virtual nominal weight.

Since manufacturing was realized with a powder-based jetting process, the maximum material grain size and the respective minimum pore size of the structures result in a smallest possible manufacturable cell size, a largest possible relative density, and a maximum height of the structures.

The smallest reliably depowderable diamond structure has a cell size of 2.2 mm and a volume fraction of 25% with a height of up to 20 mm. The pore size of this structure is 320 µm. With an average particle grain size of 16.6 µm, this corresponds to a factor of about 20. Figure 7(b) shows a cross section of this sample. A diamond structure with a cell size of 2.0 mm is depicted in Figure 7(a). Cosintered residual powder can be observed in the center of the latter image.

(A) DIAMOND STRUCTURE WITH 2.0 MM CELL SIZE

(B) DIAMOND STRUCTURE WITH 2.2 MM CELL SIZE

1mm

1mm
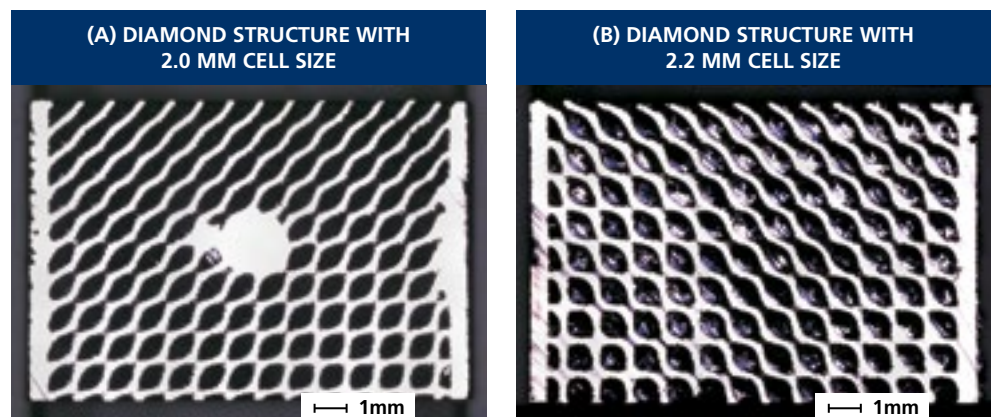
Figure 7: Diamond structure with different cell sizes at a volume fraction of 25% and a specimen height of 10 mm

Figure 8 features two diamond structures with different volume fractions. Figure 8(b) depicts a sample with a volume fraction of 55%, which shows cosintered residual powder. Figure 8(a) consists of a sample with a volume fraction of 45%, which was successfully depowdered.

(A) DIAMOND STRUCTURE WITH 45% VOLUME FRACTION

(B) DIAMOND STRUCTURE WITH 55% VOLUME FRACTION

1 mm

1 mm
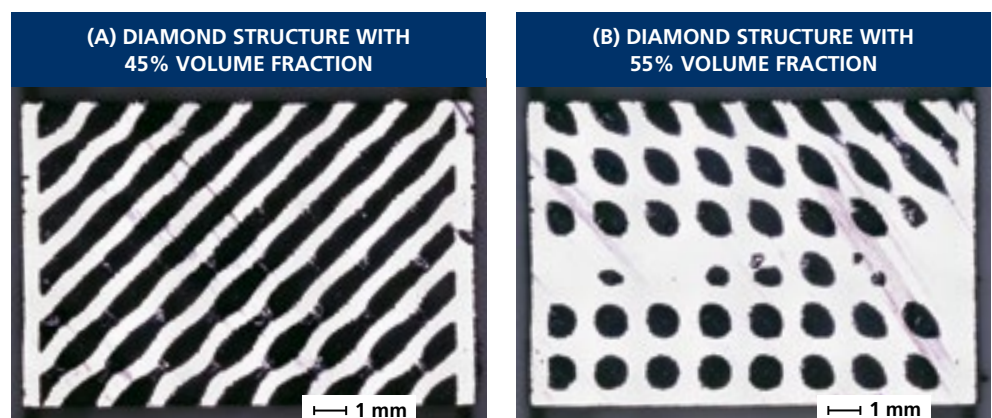
Figure 8: Diamond structure with different volume fractions at a cell size of 3.4 mm and a specimen height of 20 mm

Figure 9 depicts two split P structures with different cell sizes. The structure with a cell size of 2.2 mm in (a) shows a large area of cosintered residual powder. The structure with a cell size of 3.4 mm in (b), on the other hand, was successfully depowdered.

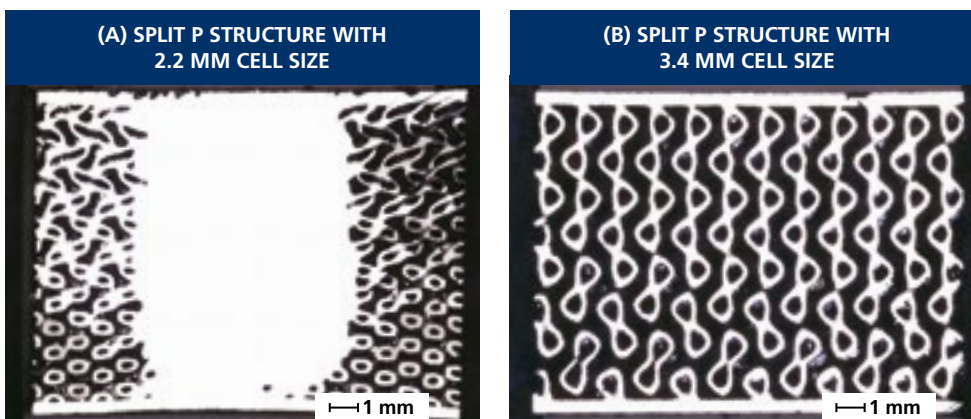*Figure 9: Split P structure with different cell sizes at a volume fraction of 25% and a sample height of 20 mm*

Figure 10 shows two gyroid structures with a cell size of 2.2 mm in (a) and a cell size of 3.4 mm in (b). It can be seen that both samples were successfully depowdered.
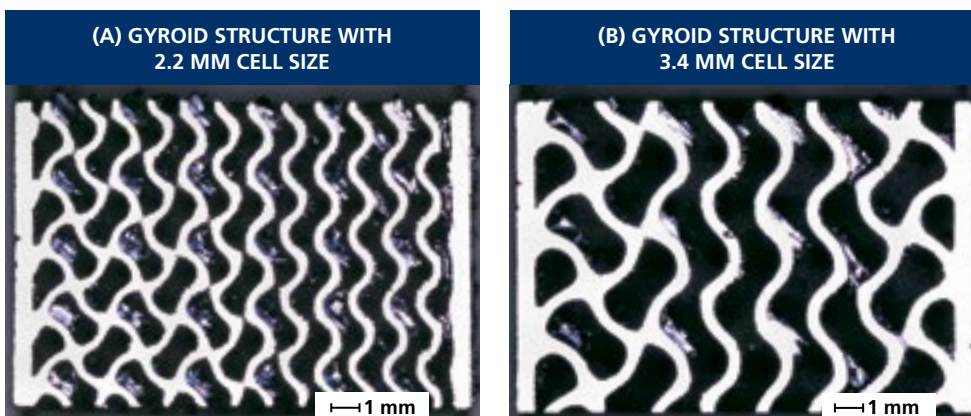

Figure 10: Gyroid structure with different cell sizes at a volume fraction of 25% and a sample height of 10 mm

6.5_MECHANICAL PROPERTIES

The mechanical properties of TPMS structures are typically characterized by the Gibson-Ashby model [AlK19]. This model allows the specification of macroscopic effective material parameters as a function of the relative density ϕ of the TPMS structure. The Young's modulus E_{TPMS} of a TPMS structure is considered here as an exemplary mechanical parameter (other parameters can be determined in a similar fashion):
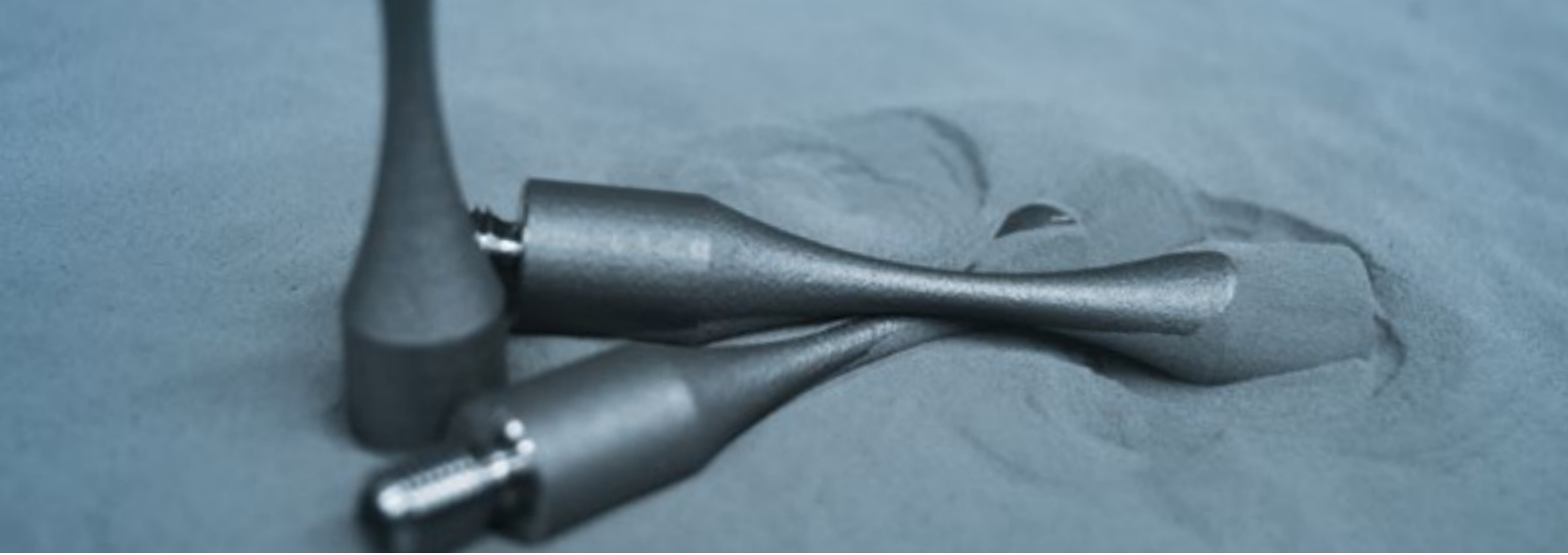
$$E_{TPMS} = C \cdot \phi^N \cdot E_{solid}$$

Here, E_{solid} stands for the Young's modulus of the solid, while C and N describe the material characterization according to Table 3. These are experimental values. Since the gyroid and diamond structures in particular provide the best effective Young's moduli for different cell sizes [AlK19], only these two structures will be considered in the following.

TPMS STRUCTURE	UNIT CELL (mm)	MATERIAL	C	N
	1.50	Titanium	12.70	1.10
Gyroid	4.00	Stainless steel	216.60	2.23
	7.00	Maraging steel	18.50	1.23
	1.50	Titanium	9.90	0.79
Diamond	4.00	Stainless steel	81.70	1.42
	7.00	Maraging steel	6.70	0.52

Table 3: Parameters for determining the Young's modulus of the gyroid and the diamond TPMS shell structure according to the Gibson-Ashby model for different unit cell sizes and materials (cf. [AlK19])

If a specific Young's modulus is required for a design, graphs such as those shown in Figure 11 are recommended to derive the required relative density. In the range of low relative densities, the diamond structure is clearly superior to the gyroid structure. Above a break-even point, which shifts as a function of relative density, the gyroid structure delivers a higher Young's modulus than the diamond structure.

TITANIUM, UNIT CELL 1.5 MM

Effective Young's modulus (GPa) vs Relative density (1)
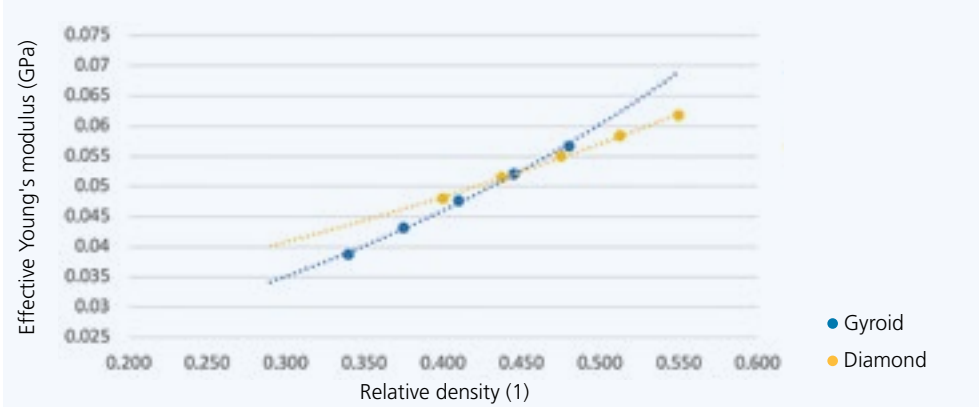
- Gyroid
- Diamond

STAINLESS STEEL, UNIT CELL 4 MM

Effective Young's modulus (GPa) vs Relative density (1)
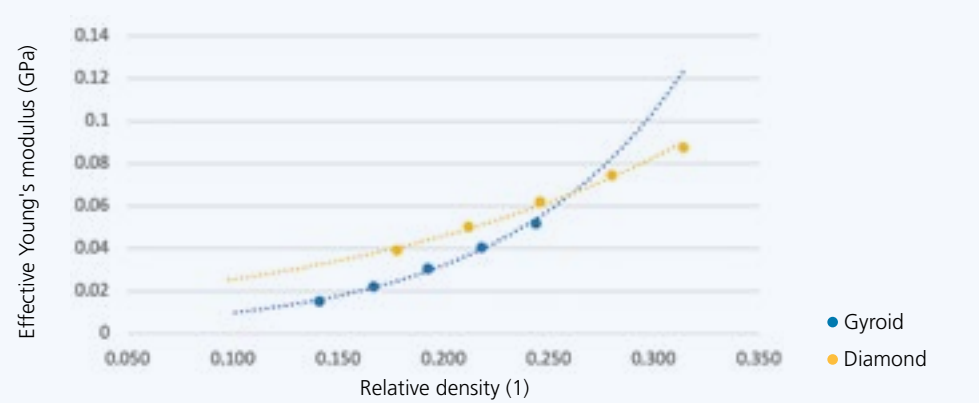
- Gyroid
- Diamond

MARAGING STEEL, UNIT CELL 7 MM

Effective Young's modulus (GPa) vs Relative density (1)

- Gyroid
- Diamond

Figure 11: Experimentally determined effective Young's moduli of the gyroid and the diamond TPMS shell structure as a function of relative density for different materials and cell sizes (data extracted from [AIK19])
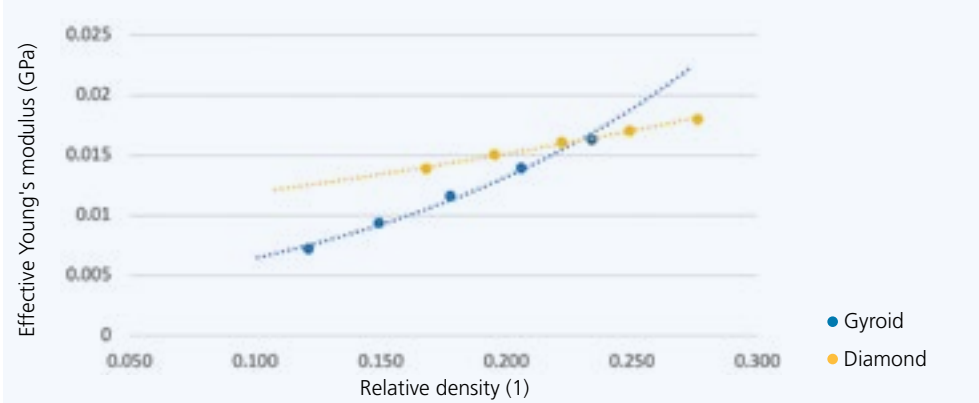
7_APPLICATIONS

7.1_SHOCK

Key question:
Why can TPMS structures be beneficial in controlled impact energy absorption?

Tunable material properties can be achieved by functionally grading the relative density of TPMS structures. Such properties include, for example, defined crash behavior and improved energy absorption [AlK19]. This is illustrated by the graded TPMS structure shown in Figure 12. The structure can be regarded as a series of connected predetermined breaking elements (similar to springs) with (from left to right) linearly decreasing strength. If an impact on the structure occurs from the right with a certain force and this force per impact area corresponds exactly to the strength, for example, of the first two elements from the right, then only these two elements will fail. If the strength distribution in the structure and the impact force are known, it is possible to predict exactly up to which layer the entire structure will collapse in a crash.

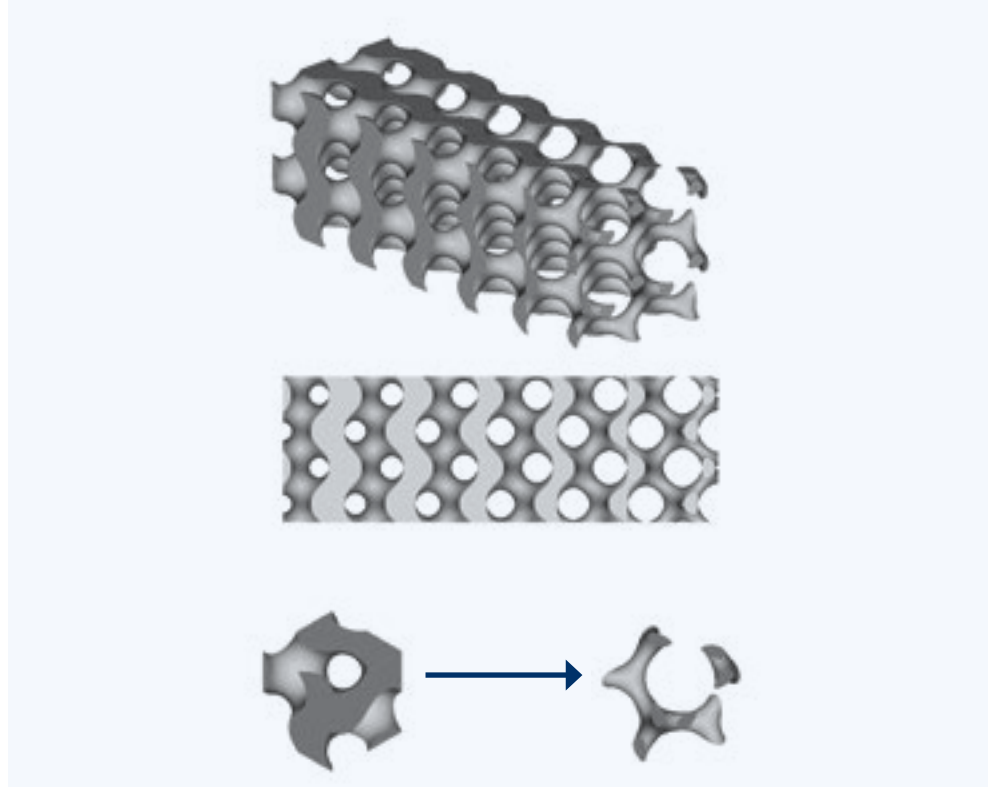**LINEARLY GRADED GYROID STRUCTURE**

Figure 12: Linear grading of the relative density of a TPMS structure from left to right from 50% to 10% (cf. [AlK19])

This behavior is illustrated in a (static) compression test using a primitive TPMS shell structure as an example (see Figure 13). The uniform structure (top row) is seen to collapse in random directions. By contrast, in the graded structure (bottom row) failure starts at the thinnest and thus weakest layer and then gradually extends to the thicker layers layer by layer, as structural strength increases with gradually increasing wall thickness.

RANDOM FAILURE OF THE LAYERS		
Uniform primitive	Sample 1, compression 17.2 mm	Sample 2, compression 17.8 mm	Sample 3, compression 24.7 mm

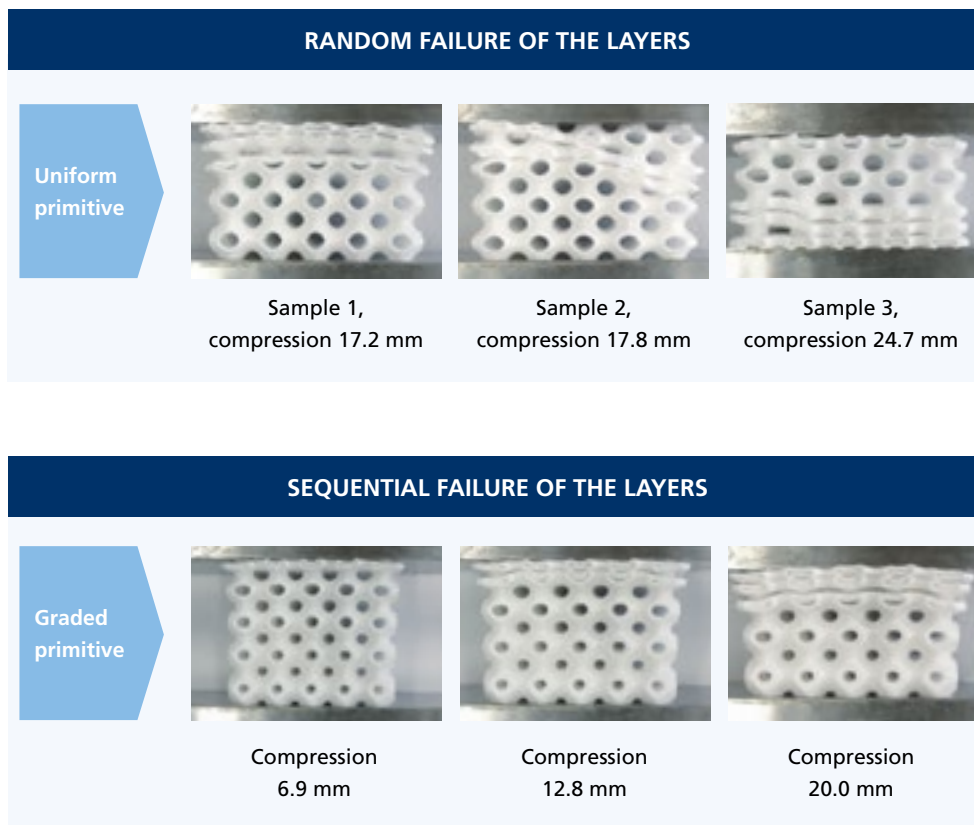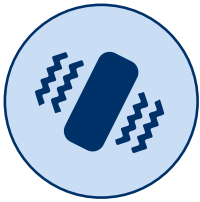| SEQUENTIAL FAILURE OF THE LAYERS		
Graded primitive	Compression 6.9 mm	Compression 12.8 mm	Compression 20.0 mm

Figure 13: Deformation behavior of primitive TPMS shell structures under compressive loading; top row: different samples, bottom row: same sample

7.2_VIBRATION

Key question:
Which TPMS structure can be used to decouple a vibrating system?

Some TPMS structures exhibit mechanical bandgap behavior, that is, they are able to completely eliminate oscillations in the corresponding frequencies. As a result, the initial frequencies and the widths of the bandgaps can be directly influenced by suitable selection of cell size and relative density. Furthermore, TPMS structures have the ability to provide structural damping even when there is no bandgap.

Elmadih et al. [Elm19] have investigated the vibrational behavior of solid and shell gyroid as well as diamond TPMS structures on the basis of simulations. The material used was Nylon-12. Figure 14 shows the smallest natural frequency for each individual structure. It can be seen that the solid gyroid structure has the lowest first natural frequency, and it is the most promising option in the context of bandgaps, as these are always found above this frequency. For this reason, only this structure will be considered in the following.

The bandgap behavior of the solid gyroid structure was also investigated [Elm19]. A bandgap is a frequency range in which the propagation of elastic waves through a periodic medium is prevented due to destructive interference of reflected waves of certain frequencies.
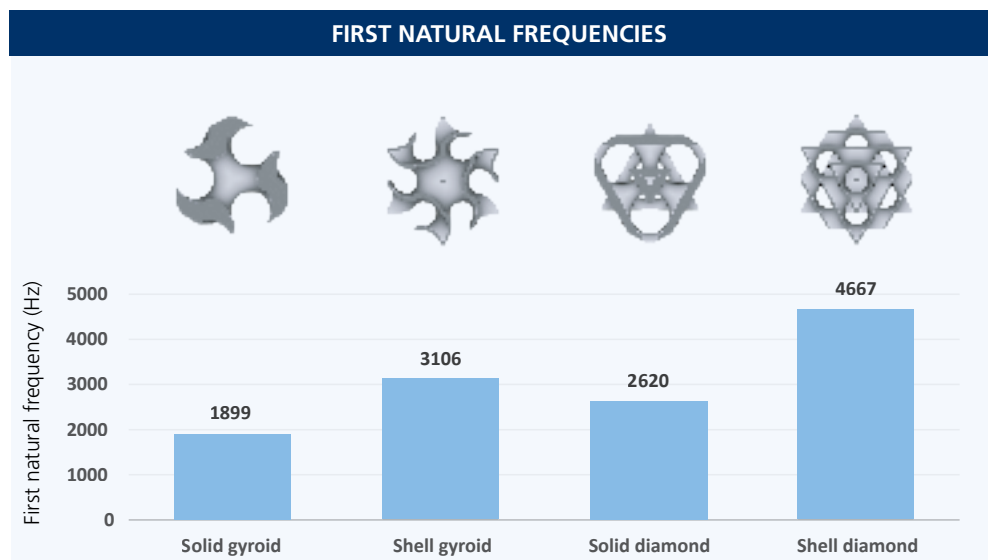
Figure 14: First natural frequencies for the solid and shell gyroid as well as diamond TPMS structures for a cell size of 15 mm and a relative density of 20% (cf. [Elm19])

FIRST NATURAL FREQUENCIES

Figure 15 depicts the dependency of the bandgaps on cell size. The 15 mm cell size has the bandgaps with the largest widths among the solid gyroid structures with cell sizes between 15 and 40 mm at a constant relative density of 20%. Smaller cell sizes have higher stiffnesses than larger cell sizes, resulting in higher bandgap frequencies.
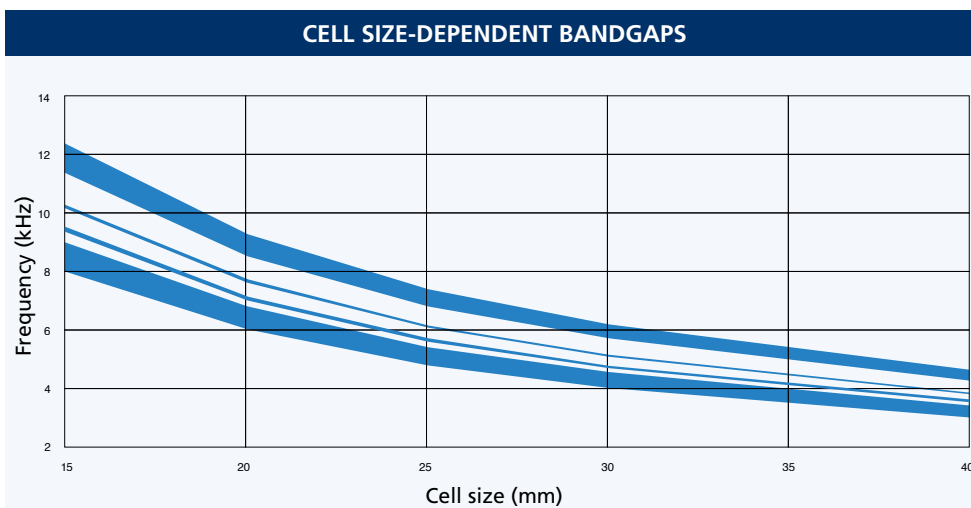
Figure 15: Bandgap dependency of a solid gyroid TPMS structure on cell size for a relative density of 20% (cf. [Elm19])

Figure 16 illustrates the dependency of the bandgaps on relative density. The bandgaps for the solid gyroid structures with relative densities between 20 and 40% are given at a constant cell size of 15 mm. The largest bandgap width is observed at a relative density of 25% with a corresponding frequency range of about 1.9 kHz.

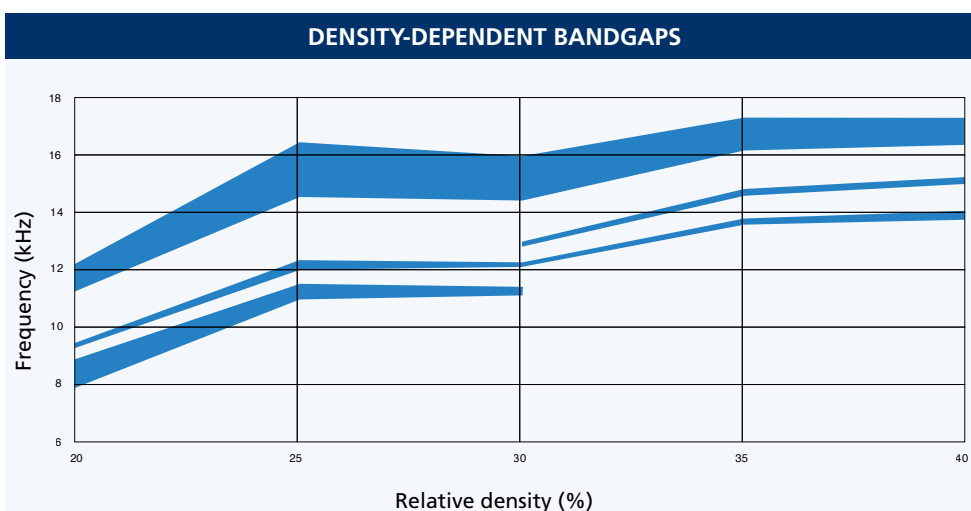*Figure 16: Bandgap dependency of a solid gyroid TPMS structure on the relative density for a cell size of 15 mm (cf. [Elm19])*

7.3_ACOUSTICS

Key question: Which TPMS structure can be used for proper sound absorption?

Two scientific works form the basis for answering this question in the context of acoustic applications of TPMS structures.

Abueidda et al. [Abu16] investigated the Neovius, IWP, and primitive TPMS shell structures for acoustic bandgaps. The investigation was purely computational using COMSOL Multiphysics, assuming PMMA to be the base material. A bandgap occurs when all incoming sound waves of one frequency are prevented from passing through the structure. Complete bandgaps are induced by destructive interference of the multiple scattered waves and the varying sound velocity within the structure. Figure 17 shows the acoustic bandgaps of the three TPMS structures investigated as a function of relative density. It is evident that higher relative densities lead to wider acoustic bandgaps.

Yang et al. [Yan20] investigated the acoustic absorption of TPMS structures manufactured by stereolithography (Formlabs Form 2, Tough resin) using the impedance tube method according to ISO 10534-2. The specimens were designed as cylinders with a diameter of 29 mm (to fit in
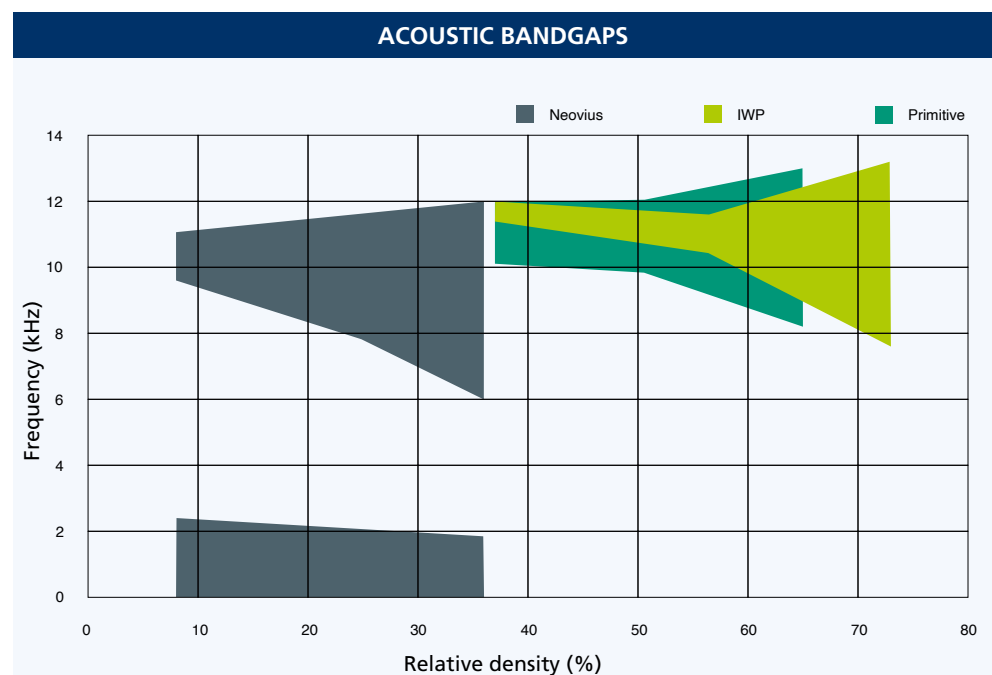

Figure 17: Acoustic bandgaps of the Neovius, IWP, and primitive TPMS shell structures as a function of relative density (cf. [Abu16])

the tube) and a wall thickness of 1 mm. Three different TPMS structures (diamond, gyroid, and primitive) were investigated by varying cell size l, relative density ϕ, and sample height h.

Figure 18 shows that the diamond structure has significantly higher absorption coefficients than the other two structures. The absorption coefficients increase with increasing relative density, while the effective absorption frequency ranges are maintained (not shown in the figure) [Yan20].
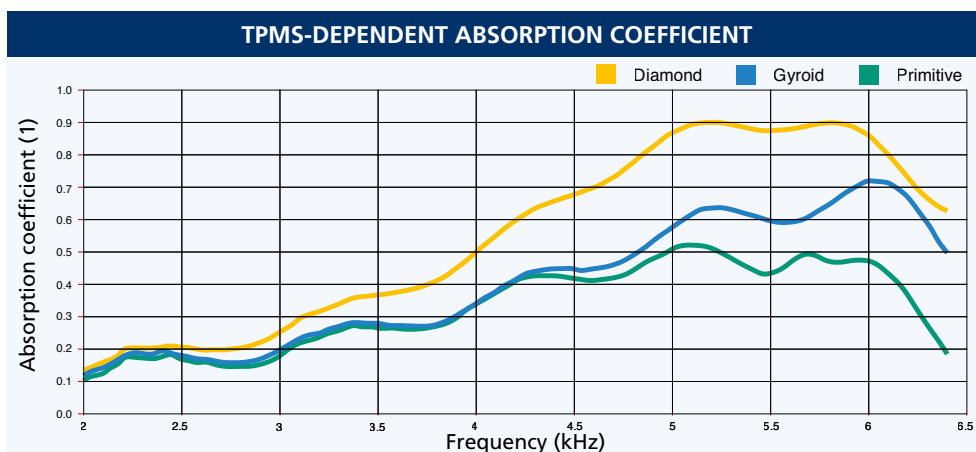
Figure 18: Comparison of the absorption coefficient of the diamond, gyroid, and primitive TPMS shell structures with $l = 5.6$ mm, $\phi = 35\%$, and $h = 11.2$ mm (cf. [Yan20])

Figure 19 shows that the absorption coefficient decreases with increasing cell size, while there is little change in the effective absorption frequency ranges. With increasing height h, the absorption curve maximum shifts to lower frequencies, while the peak value of the absorption coefficient decreases (not shown in the figure) [Yan20].

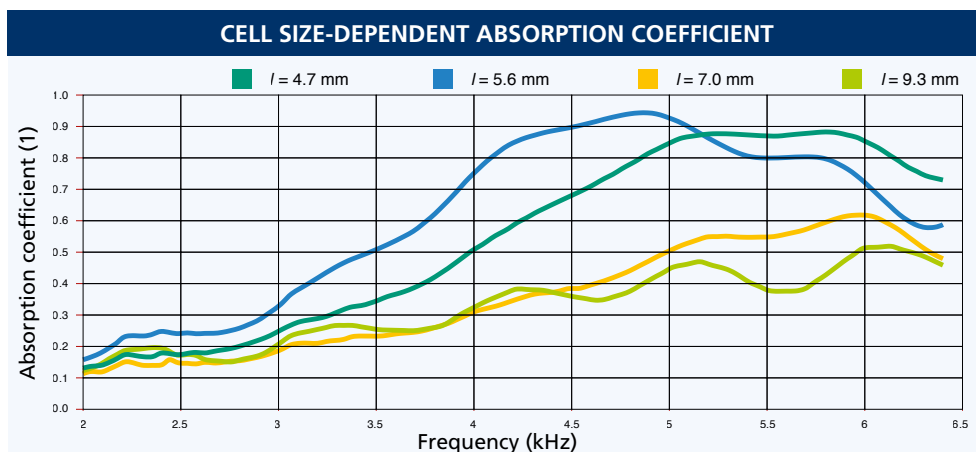*Figure 19: Comparison of the absorption coefficient of the diamond TPMS shell structure with $\phi = 35\%$ and $h = 11.2$ mm for different cell sizes (cf. [Yan20])*

7.4_HEAT TRANSFER

Key question:

Which TPMS structure can be used to realize a desired heat transfer or heat exchange?

Another use of TPMS structures is in thermal applications, where their large surface area can support heat transfer.

One of the first systematic investigations in the context of pure heat transfer was carried out by Catchpole-Smith et al. [Cat19], who experimentally analyzed the influence of cell size, wall thickness, and relative density on the heat transfer capability of gyroid, diamond and primitive TPMS shell structures. One result was the finding that as relative density increases, heat transfer also increases. In addition, TPMS shell structures with a larger minimum wall thickness at the same relative density showed increased heat transfer capability compared to those with smaller minimum wall thicknesses.

In the context of heat exchange, the bias parameter in the implicit mathematical description of TPMS, which affects the size of the two channels separated by the surface, is of importance (see Figure 20). With a bias parameter of zero, the TPMS divides the space evenly into two interpenetrating channels. With a nonzero bias, one channel expands while the other channel shrinks. However, changing the bias parameter has a negligible effect for IWP, gyroid, and primitive TPMS, for example, which can be beneficial for some applications. Fischer-Koch S TPMS
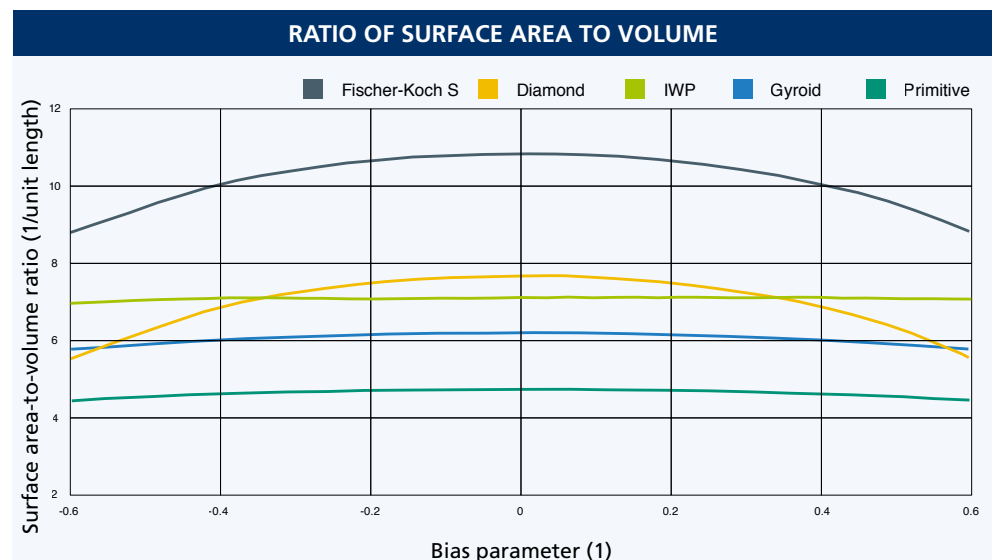

RATIO OF SURFACE AREA TO VOLUME

Figure 20: Ratio of surface area to volume as a function of the bias parameter of different TPMS bounded by a cubic volume of 1 mm³ (cf. [AIK19])

have the highest surface area-to-volume ratio among the shown TPMS and are therefore particularly well suited for use in heat exchangers.

Peng et al. [Pen19] investigated the influence of the bias parameter using fluid mechanics simulations. The results showed that heat exchangers based on TPMS shell structures with a nonzero bias parameter are particularly suitable for significant differences in the physical properties of the fluids in the two channels. For example, a fluid with higher viscosity can be directed into the expanding channel to reduce hydrodynamic resistance and a fluid with lower thermal conductivity can be directed into the shrinking channel to improve heat transfer efficiency.

Another influential parameter for heat transfer is the surface area-to-volume ratio. Figure 21 shows this ratio for the diamond, gyroid, and primitive TPMS as a function of cell size. Compared to the gyroid and the primitive structure, it is evident that the diamond structure shows the highest increase in the surface area-to-volume ratio with decreasing cell sizes. This is the most suitable of the three shown TPMS for use in heat exchangers. With a fixed bounding box, the surface area of TPMS doubles when the unit cell size is halved [Alk19].
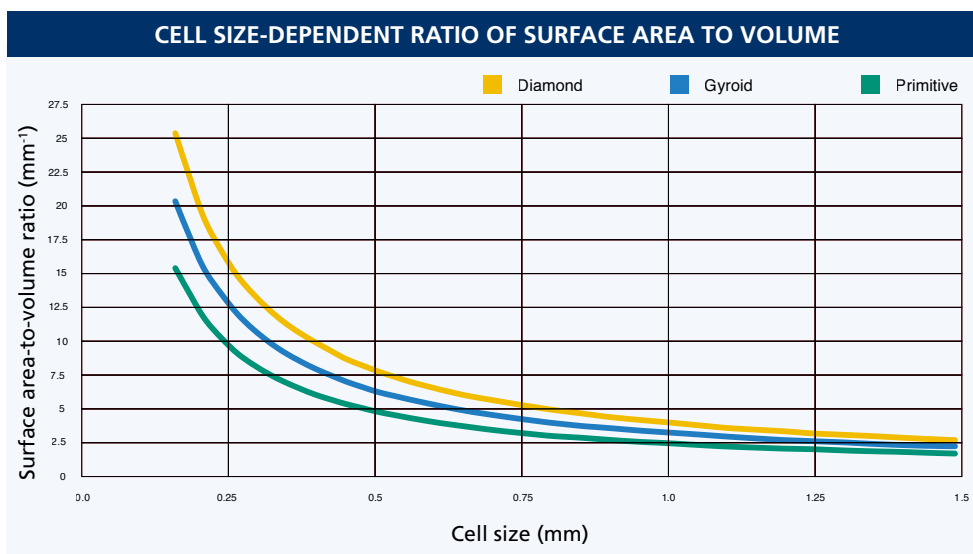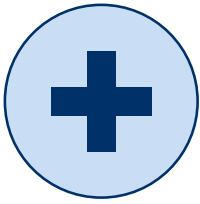

CELL SIZE-DEPENDENT RATIO OF SURFACE AREA TO VOLUME

Figure 21: Ratio of surface area to volume as a function of cell size of diamond, gyroid, and primitive TPMS (cf. [Vij18])

7.5_MEDICAL

Key question:
Why can TPMS structures be beneficial in bone scaffold and implant design?

In the medical context, TPMS structures show great potential in bone scaffold and implant design, providing a structure for bone cells to grow in. Both medical and technical demands are placed on bone scaffolds and implants. These demands mainly include high osseointegration, avoidance of stress shielding* and sufficient mechanical strength. Appropriately adjusted porosity** is capable of achieving stiffness adapted to that of the natural bone. The high surface area of TPMS structures provides a good basis for cell adhesion, while the permeability allows cell proliferation. The mathematical smoothness reduces peak stresses, which means that relatively high loads can be withstood. The corresponding design goals for the TPMS structure can be broken down to (locally) adapted porosity and functional grading of the structure [Low21].

To evaluate the suitability of TPMS structures for medical applications, it is useful to first investigate potential candidates on a simulation basis. Mechanical finite element simulations can be used to predict stiffness and strength, while computational fluid dynamics (CFD) can be used to determine permeability and cell distribution. The latter can be used to estimate the initial ingrowth behavior of bone cells, while permeability provides information about cell proliferation. Furthermore, tortuosity, which describes the degree of twisting of the structure (as well as the path that the fluid must travel through it), can be taken as an indicator in an early design stage [Gep20]. As can be seen in Figure 22, each TPMS structure shows a unique relation between porosity and permeability, while permeability increases with higher porosity.

*Difference in stiffness between implant and bone that can lead to failure.

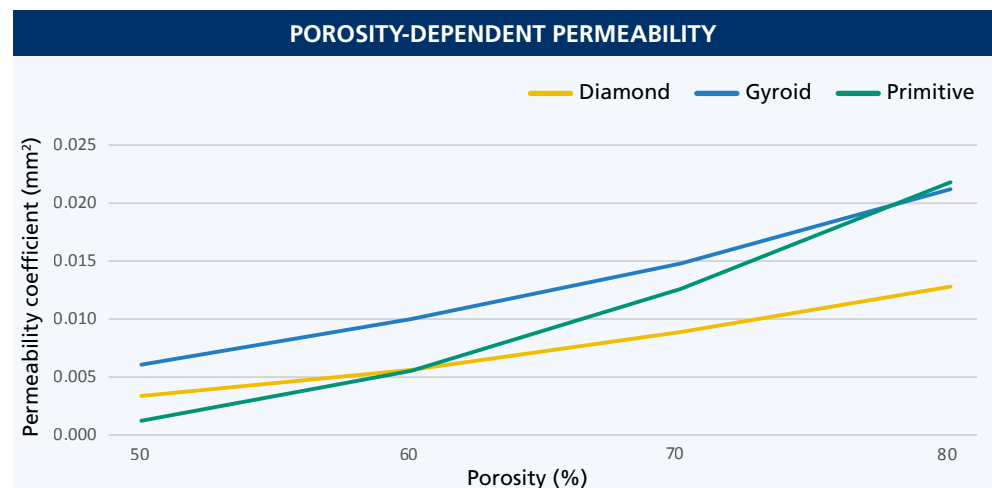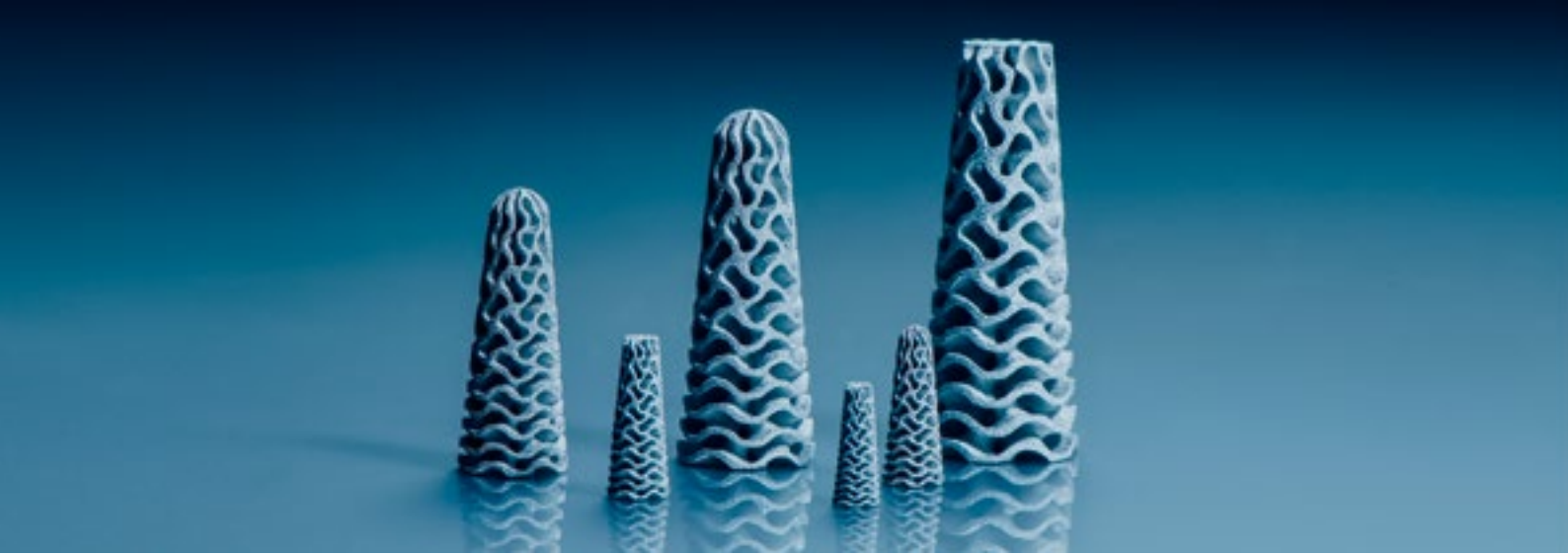**Ratio of enclosed void space to total volume of a TPMS structure.

Figure 22: Permeability coefficient as a function of porosity of the solid gyroid, schwarz, and diamond TPMS structures (cf. [Gep20])

In terms of cell adhesion, discrete phase model CFD analysis can be used to evaluate different structures [Ali19]. Results of such simulations are shown in Figure 23. Here, the double diamond 2 shell structure shows superior behavior.
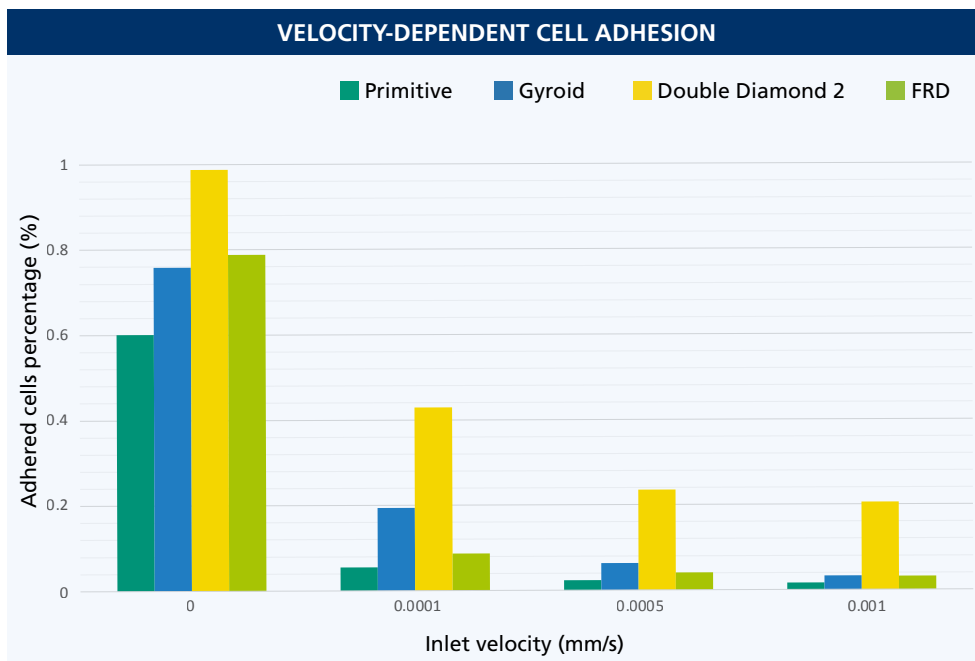
Figure 23: Percentage of adhered cells for different TPMS shell structures and inlet velocities for a porosity of 80% and a wall thickness of 0.1 mm (cf. [Ali19])

A structure suitable for the specific application should have the highest possible permeability and provide the best geometry for cell adhesion. The results of the simulations presented in Figure 23 show the advantage of a gyroid TPMS shell structure compared to a primitive one. It allows the initial adhesion of more cells while providing similar permeability at high porosity (as can be seen in Figure 22) and therefore probably the same profileration rate. This conclusion might not hold true if other (local) porosities are required to meet functional requirements. It might therefore be beneficial to use different TPMS variants in the same design.

8_SUMMARY & CONCLUSION

With the development of increasingly powerful software tools and the growing accessibility of additive manufacturing technologies to industrial companies, engineers are increasingly turning their attention to highly complex lattice structures. The favorable physical properties of structures based on TPMS make them particularly interesting for potential use in technical products. Application areas include, among others, shock, vibration, acoustics, heat transfer and the medical field.

This report comprises a literature review in the field of additively manufactured TPMS structures and fills existing gaps with own small investigations. Sections 6 and 7 contain the two main parts of this work. Section 6 focuses on the approach of this Deep Dive and section 7 investigates potential application areas for TPMS structures.

Section 6.1 begins by looking at the geometric structure of TPMS, before giving an overview of 15 selected TPMS shell structures. Section 6.2 discusses possible types of grading and transforming TPMS, illustrated by the example of the shelled gyroid structure. Geometric modeling possibilities of TPMS structures are provided in section 6.3, together with an overview of currently available software solutions for directly generating TPMS structures. Section 6.4 addresses general aspects of manufacturability and presents a small fabrication study of selected TPMS structures using the metal binder jetting process. Finally, section 6.5 introduces the Gibson-Ashby model for characterizing the mechanical properties of TPMS structures and illustrates this model using the Young's modulus as an example.

Section 7.1 describes the beneficial failure behavior of graded TPMS structures for a potential crash-related use. Section 7.2 addresses the vibrational bandgap behavior of TPMS structures. Here, the solid gyroid structure shows great potential for mechanical decoupling of a vibrating system. Section 7.3 elaborates on the acoustic damping behavior of TPMS shell structures, illustrating in particular the bandgap behavior of the Neovius, IWP, and primitive structures as well as the absorption behavior of the diamond, gyroid and primitive structures. Potential applications of TPMS structures in heat exchangers are illustrated in section 7.4. The ideal structure for a given application is seen to depend on many different parameters, with the need for more detailed investigation of corresponding interaction. Finally, section 7.5 describes the essential properties of TPMS structures which make them attractive for application in bone scaffolds and implants, discussing the porosity-dependent permeability and the rate-dependent cell adhesion of selected TPMS structures.

To conclude, this report gives engineers an overview of the physical properties of TPMS structures and provides them with methodological tools for selecting a suitable structure for their specific application. However, the individual applications need to undergo further investigations of a more in-depth nature in order to be able to create functionally optimized products.

9_REFERENCES

[Abu16]   Abueidda, D. W., Al-Rub, R. K. A., Dalaq, A. S., Lee, D. W., Khan, K. A. & Jasiuk, I. (2016). Effective Conductivities and Elastic Moduli of Novel Foams with Triply Periodic Minimal Surfaces. *Mechanics of Materials,* 95, 102–115.

[Ali19]   Ali, D. (2019). Effect of Scaffold Architecture on Cell Seeding Efficiency: a Discrete Phase Model CFD Analysis. *Computers in Biology and Medicine,* 109, 62–69.

[AlK19]   Al-Ketan, O. & Abu Al-Rub, R. K. (2019). Multifunctional Mechanical Metamaterials Based on Triply Periodic Minimal Surface Lattices. *Advanced Engineering Materials,* 21(10), 1900524.

[Cat19]   Catchpole-Smith, S., Sélo, R. R. J., Davis, A. W., Ashcroft, I. A., Tuck, C. J. & Clare, A. (2019). Thermal Conductivity of TPMS Lattice Structures Manufactured via Laser Powder Bed Fusion. *Additive Manufacturing,* 30, 100846.

[Cor17]   Corkery, R. W. & Tyrode, E. C. (2017). On the Color of Wing Scales in Butterflies: Iridescence and Preferred Orientation of Single Gyroid Photonic Crystals. *Interface Focus,* 7(4), 20160154.

[Elm19]   Elmadih, W., Syam, W. P., Maskery, I., Chronopoulos, D. & Leach, R. (2019). Mechanical Vibration Bandgaps in Surface-Based Lattices. *Additive Manufacturing,* 25, 421–429.

[Gep20]   Guerreiro, R., Pires, T., Guedes, J. M., Fernandes, P. R. & Castro, A. P. (2020). On the Tortuosity of TPMS Scaffolds for Tissue Engineering. *Symmetry,* 12(4), 596.

[Han18]   Han, L. & Che, S. (2018). An Overview of Materials with Triply Periodic Minimal Surfaces and Related Geometry: from Biological Structures to Self-Assembled Systems. *Advanced Materials,* 30(17), 1705708.

[Hub14]   Huber, N., Viswanath, R. N., Mameka, N., Markmann, J. & Weißmüller, J. (2014). Scaling Laws of Nanoporous Metals under Uniaxial Compression. *Acta Materialia,* 67, 252–265.

[Low21]   Löw, Y. M., Seibel, A. (2021). Design of Finger Joint Implants Based on Triply Periodic Minimal Surfaces. *Transactions on Additive Manufacturing Meets Medicine,* 3(1).

[Mun18]   Munsch, M., Schmidt-Lehr, M., Wycisk, E., *Ampower Insights Vol. 3* (2018). Metal Additive Manufacturing with Sinter-Based Technologies – A Deep Dive into the Emerging AM Technologies.

[Pen19]   Peng, H., Gao, F. & Hu, W. (2019). Design, Modeling and Characterization of Triply Periodic Minimal Surface Heat Exchangers with Additive Manufacturing. In *30th Annual International Solid Freeform Fabrication Symposium – An Additive Manufacturing Conference.*

[Sav19]   Savio, G., Meneghello, R. & Concheri, G. (2018). Geometric Modeling of Lattice Structures for Additive Manufacturing. *Rapid Prototyping Journal,* 24(2), 351–360.

[Vij18]   Vijayavenkataraman, S., Zhang, L., Zhang, S., Hsi Fuh, J. Y. & Lu, W. F. (2018). Triply Periodic Minimal Surfaces Sheet Scaffolds for Tissue Engineering Applications: an Optimization Approach toward Biomimetic Scaffold Design. *ACS Applied Bio Materials,* 1(2), 259–269.

[Yan20]   Yang, W., An, J., Chua, C. K. & Zhou, K. (2020). Acoustic Absorptions of Multifunctional Polymeric Cellular Structures Based on Triply Periodic Minimal Surfaces Fabricated by Stereolithography. *Virtual and Physical Prototyping,* 15(2), 242–249.

[Yu19]   Yu, S., Sun, J. & Bai, J. (2019). Investigation of Functionally Graded TPMS Structures Fabricated by Additive Manufacturing. *Materials & Design,* 182, 108021.

10_IMPRINT

Imprint

Fraunhofer Research Institution for
Additive Manufacturing Technologies IAPT
Am Schleusengraben 14
21029 Hamburg-Bergedorf
Germany
Telephone +49 40 48 40 10-500
Fax +49 40 48 40 10-999
www.iapt.fraunhofer.de
info@iapt.fraunhofer.de

A legally dependent entity of
Fraunhofer-Gesellschaft
zur Förderung der angewandten Forschung e.V.
Hansastrasse 27c
80686 Munich
Germany
www.fraunhofer.de
info@zv.fraunhofer.de

Contact

Dr.-Ing. habil. Dipl.-Ing. Arthur Seibel
Head of Bionic Function and Design
Telephone +49 40 48 40 10-748
arthur.seibel@iapt.fraunhofer.de

The Fraunhofer IAPT does not warrant that the information in this Deep Dive is correct.
No statement in this Deep Dive shall be considered as an assured prediction.
The reader should not make any decision based exclusively on the information presented.

Photo credits: all image rights are held by Fraunhofer IAPT
except for: p.10 John Wiley & Sons

Status of the Deep Dive, October 2021.